

We thank the editors for their comments which have been addressed in the revised version of the manuscript. Below are the replies (in blue) to the points raised by the Topical and Executive editors (in italic):

Topical editor comments:

*Lines 525-523: “some experiments (1-2 and 3-4) were replicated with the same imposed boundary conditions and show the same result, which ensures model reproducibility”. These additional experiments are a valuable addition to the paper, but the reader has little way of verifying the statement quoted above. One way of addressing this would be to refer to Figure 8, which shows dome diameter and apical depression width for both original and repeat experiments. Alternatively, or in addition, you could add a figure comparing key outcomes (e.g., the top view and cumulative vertical displacement) of the repeat experiments with the original ones.*

We followed these suggestions. We now refer to Figure 8 in the text and added a new figure in the supplementary material that shows the top view and cumulative vertical displacement of the replicated experiments to be compared with those in Figure 7. Please note that we also corrected an error in Figure 7 changing the term “graben” with “depression” as it is in the text.

*The newly added conclusion “the relation that relates the magmatic source depth with the surface parameters of resurgent domes is independent by the source eccentricity, similarly to what already verified for sub-circular intrusions” is important; however, as written, is grammatically incorrect. Please rephrase.*

The sentence has been rewritten.

Executive editor comments:

*Many thanks for your revised manuscript. I am satisfied that you have addressed the comments raised by the reviewers, as indicated before. However, looking at the manuscript as a whole, there are some issues with the level of English writing. We would request that you go through the manuscript once more to identify and address these issues, potentially with the help of a native English speaker. A clearly written paper will increase its impact, so hopefully this process will be helpful in the long run.*

The manuscript has been carefully revised and the level of English writing has been improved.

Sincerely,

The Corresponding Author

Stefano Urbani

# 1 Estimating the depth and evolution of intrusions at resurgent 2 calderas: Los Humeros (Mexico)

3 Stefano Urbani<sup>1</sup>, Guido Giordano<sup>1,2</sup>, Federico Lucci<sup>1</sup>, Federico Rossetti<sup>1</sup>, Valerio Acocella<sup>1</sup>,  
4 Gerardo Carrasco- Núñez<sup>3</sup>

5 <sup>1</sup>Dipartimento di Scienze, Università degli Studi Roma Tre, L.go S.L. Murialdo 1, I-00146 Rome, Italy

6 <sup>2</sup>CNR - IDPA c/o Università degli Studi di Milano, Via Luigi Mangiagalli, 34, 20133 Milano

7 <sup>3</sup>Centro de Geociencias, Universidad Nacional Autónoma de México, Campus UNAM Juriquilla, 76100, Queretaro,  
8 Mexico

9 *Correspondence to:* Stefano Urbani (stefano.urban@uniroma3.it)

10 **Abstract.** Resurgent calderas ~~represent~~ ~~are~~ ~~excellenta~~ targets ~~with high potential~~ for geothermal exploration, as they  
11 are associated with the shallow emplacement of magma, resulting in ~~a~~ widespread and long lasting hydrothermal  
12 activity. ~~Therefore, evaluating the thermal potential of resurgent calderas may provide important insights for geothermal~~  
13 ~~exploitation.~~ Resurgence is classically attributed to the uplift of a block or dome resulting from the inflation of the  
14 collapse-forming magma chamber due to the intrusion of new magma. The Los Humeros volcanic complex (LHVC;  
15 Mexico), consist~~ing~~ of two nested calderas: ~~the outer~~ ~~and older~~ Los Humeros ~~formed at 164 ka~~ and the inner,  
16 ~~resurgent,~~ Los Potreros, ~~formed at 69ka. The latter is resurgent and currently the site of an active and exploited~~  
17 ~~geothermal field (63MWe installed).~~ ~~represents~~ ~~is~~ ~~an area of high interest for geothermal exploration to optimize the~~  
18 ~~current exploitation of the active geothermal field.~~ Here we aim at better defin~~ing~~ the characteristics of the resurgence  
19 in Los Potreros, by integrating field work with analogue models, evaluating the spatio-temporal evolution of the  
20 deformation and the depth and extent of the intrusions responsible for the resurgence ~~and~~ which may represent also the  
21 local heat source(s).

22 Structural field analysis and geological mapping show that Los Potreros ~~area~~ ~~caldera floor~~ is characterized by several  
23 lava domes and cryptodomes (with normal faulting at the top) that suggest multiple deformation sources localized in  
24 narrow areas.

25 The analogue experiments simulate the deformation pattern observed in the field, consisting of magma intrusions  
26 pushing a domed area ~~developing an~~ ~~with~~ apical depression. To define the possible depth of the intrusion responsible for  
27 the observed surface deformations, we apply tested ~~established~~ relations for elliptical sources to our experiments with  
28 sub-circular sources. We found that these relations are independent ~~from~~ ~~of~~ the source and surface dome eccentricity  
29 and suggest that the magmatic sources ~~responsible for~~ ~~inducing~~ the deformation in Los Potreros are ~~present~~ ~~located~~ at  
30 very shallow depths (hundreds of meters), which is in agreement with the well data and field observations. We ~~therefore~~  
31 propose that the recent deformation at LHVC is not a classical resurgence associated with the bulk inflation of a deep  
32 magma reservoir; rather this is related to the ascent of shallow (<1 km) multiple magma bodies. A similar multiple  
33 source model of the subsurface structure has been also proposed for other calderas with an active geothermal system  
34 (Usu volcano, Japan) suggesting that the model proposed may have ~~a~~ wider applicability.

## 35 1 Introduction

36 Caldera resurgence consists of the post-collapse uplift of part of the caldera floor. Resurgence has been described in  
37 several calderas worldwide (Smith and Bailey, 1968; Elston, 1984; Lipman, 1984 and references therein), representing a  
38 frequent step in caldera evolution. Several mechanisms ~~have been invoked that to~~ trigger resurgence ~~have been invoked~~,

39 including the pressurization of the hydrothermal system (Moretti et al., 2018), regional earthquakes (Walter et al.,  
40 2009), and magmatic intrusion (Kennedy et al. 2012). Discriminating the contributions to the observed uplift of each of  
41 these mechanisms is often challenging (Acocella, 2014). However, despite the possible hydrothermal and tectonic  
42 contributions, field observations in eroded resurgent calderas (e.g. Tomochic, Swanson and McDowell, 1985; Kutcharo,  
43 Goto and McPhie 2018; Turkey Creek, Du Bray and Pallister, 1999) coupled with the long timescale of the uplift of the  
44 caldera floor (from tens to thousands years), suggest that the intrusion of magmatic bodies is the prevalent mechanism  
45 for resurgence.

46 Resurgence is commonly attributed to the emplacement of silicic magmas at different depth levels under limited  
47 viscosity contrasts with regard to the previously emplaced magma (Marsh, 1984; Galetto et al., 2017). However, though  
48 rare, resurgence may be also triggered by the injection of more primitive magma (Morán-Zenteno et al., 2004; Kennedy  
49 et al., 2012) or by the emplacement of basaltic sills, as recently documented at the Alcedo caldera (Galapagos; Galetto  
50 et al., 2019). The shape of the intracaldera resurgent structures is variable, being characterized by elliptical domes with  
51 longitudinal graben(s) at the top (e.g. Toba; De Silva et al., 2015; Snowdonia, Beavon, 1980; Timber Mountain,  
52 Christiansen et al., 1977) or, less commonly, by sub-circular domes (e.g. Cerro Galan, Folkes et al., 2011; Long Valley,  
53 Hildreth et al., 2017; Grizzly Peak, Fridrich et al., 1991) with both longitudinal grabens (Long Valley) or concentric  
54 fault blocks (Grizzly Peak) at their top.

55 Whatever is the shape, resurgence is often associated with hydrothermal and ore forming processes, since the circulation  
56 pattern and temperature gradients of geothermal fluids are structurally-controlled by the space-time distribution of faults  
57 and fractures and by the depth and shape of the magmatic sources (e.g. Guillou Frotier et al., 2000; Prinbow et al.,  
58 2003; Stix et al., 2003; Mueller et al., 2009; [Giordano et al., 2014](#)). Therefore, the characterisation of the magma that  
59 drives resurgence (location, depth and size) and of the factors controlling the release of ~~the~~ heat (permeability, fracture  
60 patterns, and fluid flow) have important implications for the exploration and exploitation of renewable geothermal  
61 energy resources. In particular, the estimation of the location, depth and geometry of the magmatic sources is crucial to  
62 define the geothermal and mineral potential of resurgent calderas, allowing an economically sustainable exploration and  
63 exploitation of their resulted natural resources.

64 The depth and size of the magmatic sources influences the deformation style of the resurgence at the surface (Acocella  
65 et al., 2001). Deep sources (i.e. depth/diameter ratio  $\sim 1$  assuming a spherical source) are associated to resurgent blocks  
66 (e.g. Ischia and Pantelleria, Acocella and Funicello, 1999; Catalano et al., 2009), whereas shallower sources (i.e.  
67 depth/diameter ratio  $\sim 0.4$ ) to resurgent domes (e.g. Valles and Yenkahe, Kennedy et al., 2012; Brothelande et al., 2016).  
68 Moreover, uplift rates may change by one order of magnitude from  $\sim 1$  to  $\sim 10$  cm per year (e.g. Yellowstone and Iwo  
69 Jima, Chang et al., 2007; Ueda et al., 2018). Nevertheless, despite showing different uplift styles and rates, these natural  
70 examples share a common feature that is a coherent uplift of the caldera floor.

71 ~~This scenario differs from the occurrence of~~ A different style of deformation patterns is observed at calderas  
72 characterized by the widespread and delocalized uplift of several minor portions of the caldera floor, due to associated  
73 with the shallow emplacement of lava domes and/or sills and cryptodomes, as observed at Usu volcano (Japan,  
74 Matsumoto and Nakagawa, 2010; Tomya et al., 2010). Such deformation pattern suggests A ~~a~~ different depth(s) and  
75 extent(s) of the ~~responsible magma~~ source(s) and, consequently, a different subsurface structure of the volcano is  
76 ~~therefore suggested~~. A better assessment of the subsurface structure in ~~such this type of calderasese cases~~ has crucial  
77 implications for geothermal exploration ~~in order to maximize the geothermal production~~.

78 The Los Humeros Volcanic Complex (LHVC, Mexico) is an important geothermal target area, consisting of two nested  
79 calderas: Los Humeros (the outer, larger and older one; [164 ka](#)) and Los Potreros (the inner, smaller and younger one;

80 69 ka) (Fig. 1). The latter is characterized by the resurgence of its floor, ~~which was previously~~ interpreted ~~as-to be~~ due  
81 to ~~uplift processes related to~~ the inflation of ~~thea magma chamber responsible for the collapse, with its top at ca 5 km~~  
82 ~~depthseveral km\_deep magma chamber~~ (Norini et al., 2015, 2019).

83 This paper aims at (1) evaluating the depth of the intrusion(s) ~~responsible for~~ inducing the uplift in the LHVC area; (2)  
84 explain the spatio-temporal evolution of the observed deformation of the caldera floor and (3) test the validity of the  
85 linear relationship between the surface deformation structures and depth of elliptical sources (Brothelande and Merle  
86 2015) for sub-circular sources. To achieve these goals, we integrate results from structural field investigations carried  
87 out within the Los Potreros caldera with those derived from analogue experiments specifically designed to constrain the  
88 depth of the deformation source(s) in volcanic caldera environments. The obtained results show that: (1) the relation  
89 between the source depth and surface deformation structures is independent ~~from-of~~ the source eccentricity; (2) the  
90 LHVC is characterized by discontinuous and small-scale (areal extent  $\sim 1 \text{ km}^2$ ) surface deformations generated from  
91 multiple and shallow-emplaced ( $< 1 \text{ km}$  depth) magmatic bodies. These results should be taken into account for the  
92 planning of future geothermal operations at the LHVC and in other calderas showing similar surface deformation.

## 93 2 Geological-structural setting

94 LHVC is located at the eastern termination of the Trans Mexican Volcanic Belt (TMVB, see inset in Fig. 1). The TMVB  
95 is the largest Neogene volcanic arc in Mexico ( $\sim 1000 \text{ km}$  long and up to  $\sim 300 \text{ km}$  wide), commonly associated with the  
96 subduction of the Cocos and Rivera plates beneath the North American plate along the Middle American trench (Ferrari  
97 et al., 2012, and references therein). The LHVC consists of two nested calderas formed during the Pleistocene: the outer  
98  $18 \times 16 \text{ km}$  Los Humeros caldera and the inner  $10 \times 8 \text{ km}$  Los Potreros caldera (Fig. 1, Ferriz and Mahood, 1984;  
99 Norini et al., 2015; Carrasco-Núñez et al., 2017b).

100 Based on updated stratigraphic and geochronological information, the evolution of the LHVC can be divided into three  
101 main eruptive stages (Table 1, Carrasco-Núñez et al., 2017b, 2018). Pre-caldera volcanism extended between ca. 700  
102 and 164 ka (U-Th and  $^{39}\text{Ar}/^{40}\text{Ar}$  datings in Carrasco-Núñez et al., 2018), showing evidence for an extended building  
103 phase leading to the establishment of the large volume rhyolitic reservoir, which fed several lava domes erupted to the  
104 western border of the Los Humeros Caldera. A Caldera stage started at ca. 164 ka (U-Th and  $^{39}\text{Ar}/^{40}\text{Ar}$  ages, Carrasco-  
105 Núñez et al., 2018), with the eruption of the  $\geq 115 \text{ km}^3$  ~~(dense rock equivalent volume)~~ Xaltipan ignimbrite that  
106 triggered the collapse of the Los Humeros caldera. This was followed by a Plinian eruptive episodic sequence,  
107 characterized by the emplacement of several rhyodacitic pumice fallout layers grouped as the Faby Tuff (Ferriz and  
108 Mahood, 1984). The Caldera stage ended with the eruption of the  $15 \text{ km}^3$  ~~(dense rock equivalent volume)~~ Zaragoza  
109 rhyodacite-andesite ignimbrite at  $69 \pm 16 \text{ ka}$  ( $^{39}\text{Ar}/^{40}\text{Ar}$  ages, Carrasco-Núñez et al., 2018) associated with the collapse of  
110 the nested Los Potreros caldera.

111 A post-caldera stage ( $< 69 \text{ ka}$ ) is interpreted by Carrasco-Núñez et al. (2018) as composed by two main eruptive phases:  
112 (i) a late Pleistocene resurgent phase, characterized by the emplacement of silica-rich small domes and disperse  
113 explosive activity within Los Potreros caldera, followed by (ii) Holocene basaltic to trachytic monogenetic ~~volcanism~~  
114 ~~both inside and intra-caldera and~~ at the caldera-rim, ~~volcanism~~. This eruptive behaviour indicates a change in the  
115 configuration of the magmatic plumbing system ~~with respect compared~~ to the ~~early~~ caldera stage of Los Humeros, ~~which~~  
116 ~~has been referred to an-when a single-unique~~, large and homogenized magma reservoir ~~was in existence~~ (e.g. Ferriz and  
117 Mahood, 1984; Verma, 1985). ~~Rather, it is instead in favour of a~~ Volcanological and petrological data indicate that the  
118 ~~post-caldera volcanism is associated with a~~ heterogeneous multi-layered system vertically distributed ~~in the~~ within the  
119 crust, with a deep (ca.  $30 \text{ km}$  depth) basaltic reservoir feeding progressively shallower and smaller distinct stagnation

120 layers, pockets and batches up to very shallow conditions (ca. 3km) (Lucci et al., ~~under review~~2020), in agreement with  
121 recent conceptual models for magma reservoirs under caldera systems (e.g. Cashman and Giordano, 2014).

122 During the early resurgent phase of the post-caldera stage, rhyolitic domes were emplaced along the northern rim and  
123 within of the Los Humeros caldera, Available ages span and within the caldera at between 44.8±1.7 ka (U-Th ages) and  
124 50.7±4.4 ka ( $^{39}\text{Ar}/^{40}\text{Ar}$  ages), respectively (Carrasco-Núñez et al., 2018). This effusive activity was followed by several  
125 explosive eruptions, which originated a dacitic air fall called Xoxoctic Tuff (0.6 km<sup>3</sup>, Ferriz and Mahood, 1984) and a  
126 pyroclastic sequence that includes an explosive breccia and pyroclastic flow deposits comprising the Llano Tuff (Ferriz  
127 and Mahood 1984; Willcox, 2011).

128 The Holocene ring-fractures fed bimodal magmatism characterized by both explosive and effusive activity, producing  
129 several lava flows and domes, as well as ~~the~~ ca. 7 ka (C-14 age, Dávila-Harris and Carrasco-Núñez, 2014) Cuicuiltic  
130 Member during periods of dominant explosive activity. ~~It~~The Cuicuiltic Member consists of alternating pumices and  
131 scoriae erupted during contemporaneous sub-Plinian to Strombolian activity from multiple vents located mostly along  
132 the inner part of the caldera and outer caldera ring faults (Dávila-Harris and Carrasco-Núñez, 2014). During this phase,  
133 less evolved lavas (trachyandesite to basalt) were erupted within and outside the Los Humeros-Potreros caldera,  
134 including the olivine-bearing basaltic lava that fills the previously formed Xalapasco crater (Fig. 1). Trachytic lava  
135 flows are the most recent activity recorded products in the area, with an age of ca. 2.8 ka (C-14 age, Carrasco-Núñez et  
136 al., 2017b).

137 The reconstruction of the shallow stratigraphy within the Los Potreros caldera is chiefly derived from the analysis of  
138 available well-logs (Figs. 2a-b Carrasco-Núñez et al., 2017a, b). Overall, the post-caldera units are lithologically  
139 dominated by lava flows resting on ignimbrite deposits emplaced during the caldera stage. Ignimbrites of the caldera  
140 stage rest in turn on a thick sequence dominated by andesite lavas dated at ca. 1.4-2.8 Ma ( $^{39}\text{Ar}/^{40}\text{Ar}$  ages, Carrasco-  
141 Núñez et al., 2017a). The subsurface geometry of the pre- and syn-caldera products is shown in Figs. 2a-b, where the in-  
142 depth geometry of the different magmatic products are cross-correlated and projected along the N-S and E-W direction,  
143 respectively. The N-S projection shows a constant depth of the top surface of the pre-caldera andesites that is associated  
144 with a highly variable depth (down to -400 m) of the top surface of the syn-caldera Xaltipan ignimbrite. The W-E  
145 projection shows a higher depth variability of both the top surface of the pre-caldera group (down to -500 m between H-  
146 19 and H-25 wells) and that of the Xaltipan ignimbrite (down to -400 m between H-19 and H-10 wells). Basaltic and  
147 rhyolitic-dacitic lavas occur at various depths (Carrasco-Núñez et al., 2017a); rhyolitic-dacites are located mostly at the  
148 base (H-20 and H-26 wells) or within (H-05 well) the caldera group or the old andesite sequence (H-25 and H-19  
149 wells). Basalts are located only within the pre-caldera andesite sequence, both at its base (in contact with the limestone  
150 basement; H-5 and H-8 wells) and at its top (in contact with the base of the caldera sequence; H-10 well). These  
151 bimodal lava products, showing an irregular lateral distribution, have been interpreted as subaerial (Carrasco-Núñez et  
152 al., 2017a).

153 The structural architecture of the LHVC is controlled by a network of active extensional fault systems, made of NNW-  
154 SSE, N-S, NE-SW and E-W striking fault strands cutting across the Los Potreros caldera floor. The following main  
155 faults were recognised (Norini et al., 2015, 2019; Calcagno et al., 2018) (Fig.1): (i) Maxtaloya (NNW-SSE striking), (ii)  
156 Los Humeros and Loma Blanca (N-S striking), (iii) Arroyo Grande (NE-SW striking), (iv) Las Viboras and Las Papas  
157 (E-W striking). Such active fault systems are interpreted as due to the recent/active resurgence of the Los Potreros  
158 Caldera. Since the faults do not show continuity beyond the caldera border, their scarps decrease in height towards the  
159 periphery of the caldera and the dip-slip displacement vectors show a semi-radial pattern (Norini et al., 2015).

160 The source of the areal uplift has been inferred to be the inflation of a saucer or cup shaped deep magmatic source  
161 elongated NNW-SSE, up warping a 8 x 4 km resurgent block, centred in the SE portion of the caldera, delimited to the  
162 W by the NNW-SSE main faults, and toward the north, east and south by the caldera rim (Fig.1, Norini et al., 2015,  
163 2019).

164 The seismic activity between 1994-2017 is clustered along the Loma Blanca, Los Humeros and Arroyo Grande faults  
165 (Lermo et al., 2018; Fig. 1). Most of the earthquakes show a magnitude ( $M_w$ ) between 1 and 2.5 and have been mainly  
166 interpreted as induced by the geothermal exploitation activity (injection of fluids and hydrofracturing; Lermo et al.,  
167 2018). Four major earthquakes ( $M_w$ = 3.2, 3.6, 3.9 and 4.2, at a depth of 1, 4, 2.2 and 1.8 km, respectively) have also  
168 been reported, with focal depths close to the trace of the active faults (Loma Blanca and Los Humeros, Fig.1). Such  
169 major earthquakes have been interpreted as triggered by fault reactivation due to fluid/brine circulation injected from  
170 geothermal wells (Lermo et al., 2018).

### 171 3 Methods

172 ~~The scientific rationale adopted in t~~This study is based on structural field work combined with analogue models aimed  
173 ~~to at~~ constraining the depth of the deformation sources in the caldera domain. We also tested if the relation that  
174 constrains the depth of the source deformation from surface parameters adopting elliptical sources (Brothelande and  
175 Merle 2015) is verified also for sub-circular sources.

#### 176 3.1 Structural field work

177 Structural field work was carried out on the post-caldera (~~late-Late~~ Pleistocene to Holocene) deposits to characterise the  
178 surface deformation related to the recent activity of the Los Potreros caldera and constrain the morphotectonic  
179 fingerprints of the resurgence to evaluate its source and areal extent. The geometry and distribution of the observable  
180 faults and joints were defined at the outcrop scale by measuring their attitudes (strike and dip; right-hand rule) and  
181 spacing. Fault kinematics was assessed through classical criteria on slickensides fault surfaces, such as Riedel shears,  
182 growth ~~fibres~~ and sheltering trails (Doblas, 1998). The published geological map (Carrasco-Núñez et al., 2017b) and  
183 geothermal well data ~~has have~~ been used (Carrasco-Núñez et al., 2017a) to correlate the surface structures at a broader  
184 scale. The relationships between faulting and alteration have been ~~been~~ assessed (e.g. Giordano et al. 2013; Vignaroli et  
185 al. 2013, 2015)

#### 187 3.2 Analogue models: experimental set-up and scaling

188 Five experiments were undertaken ~~simulating to simulate~~ the ascent of a viscous sub-circular intrusion in a brittle  
189 overburden to test the validity of existing relationships between the depth of elliptical intrusions and the observed  
190 surface deformation (Brothelande and Merle, 2015). The experimental set-up (Fig. 3) consists of a 31 × 31 cm glass box  
191 filled with a sand pack (crust analogue) of variable thickness ( $T$ , of 10, 30 and 50 mm, respectively). In each experiment  
192 we imposed a layering using a non-cohesive marine sand below a layer of crushed silica sand (grain size = 40-200  $\mu\text{m}$ ,  
193 cohesion = 300 Pa), fixing the thickness ratio of the two layers ( $T_u/T_l$ ) to 1, to simulate the stratigraphy in Los Potreros  
194 (stiffer post caldera lava flows above softer and less cohesive ignimbrite deposits emplaced during the caldera collapse  
195 stage). At the base of the sand pack, a piston, controlled by a motor, pushes upward the silicone (magma analogue)  
196 placed inside a cylinder 8 cm in diameter. The injection rate is fixed for all the experiments to 2 mm/hr and each  
197 experiment was stopped at the onset of the silicone extrusion. Both sand and silicone physical properties are listed in  
198 Table 2.

199 At the end of each experiment, the surface has been covered with sand to preserve their final topography and ~~were-was~~  
200 wetted with water for cutting in sections to appreciate the subsurface deformation. Such sections were used to measure  
201 the mean dip of the apical depression faults ( $\theta$ ) induced by the rising silicone. A digital camera monitored the top view  
202 deformation of each experiment at 0.02 fps and a laser scanner, placed next to the camera, provided high-resolution data  
203 (maximum error  $\pm 0.5$  mm) of the vertical displacement ~~that was used~~ to measure in detail the geometrical features of  
204 the deformation i.e. dome diameter ( $L_d$ ), apical depression width ( $L_g$ ) and dome flank mean dip ( $\alpha$ ). According to the  
205 Buckingham- $\Pi$  theorem (Merle and Borgia 1996 and references therein), our models need 7 independent dimensionless  
206 numbers to be properly scaled (i.e. 10 variables minus three dimensions; Table 2). Such dimensionless numbers can be  
207 defined as the ratios ( $\Pi$ ) listed in Table 3. Some values of  $\Pi_5$ , representing the ratio between the inertial and viscous  
208 forces, are very small both in nature and experiments ( $1.3 \times 10^{-20}$  and  $6.1 \times 10^{-10}$ , respectively), indicating that the  
209 inertial forces are negligible ~~with respect~~compared to the viscous forces in both cases.

## 210 **4 Results**

### 211 **4.1 Structural geology**

212 The outcropping post-caldera lithologies within the Los Potreros Caldera consist of: (1) the Cuicuiltic Member, which  
213 blankets most of the surface of the upper half of the studied area; (2) basaltic lava flows filling the Xalapasco crater and  
214 the NW portion of the caldera; and (3) trachyandesitic and trachytic lava domes and thick flows extending in the  
215 southern half of the caldera and rhyolitic domes in its central part (Fig. 4). Field work documented that the more  
216 evolved lavas form five nearly N-S trending elliptical domes, distributed in both sides of the Los Humeros Fault (Figs. 4  
217 and 5a): (i) a 2 km long  $\times$  1.2 km wide trachytic dome located to the west of the Maxtaloya and Los Humeros faults, (ii)  
218 a 1  $\times$  0.7 km trachyandesitic dome located in a northeast area of the Maxtaloya fault, and (iii) one trachyandesitic and  
219 two obsidian smaller domes (0.4  $\times$  0.2 km) to the eastern side of the Los Humeros Fault (LH-11 in Fig. 4).

220 Field work concentrated on the three main uplifted areas corresponding to the surface expression of the Loma Blanca,  
221 Arroyo Grande and Los Humeros faults (labelled LH1-2, LH9 and LH10 respectively in Fig. 4). The observed  
222 structures in these uplifted areas (joints and faults) affect the deposits of the post-caldera phase. Based on field  
223 evidence, we also propose a revised interpretation of the surface structures identified by previous studies (Norini et al.,  
224 2015, 2019), distinguishing between lineaments (morphological linear scarps, with no measurable fault offsets and/or  
225 alteration at the outcrop scale), active and inactive faults, instead associated with measurable fault offsets and with  
226 active or fossil alteration, respectively (Fig. 4). We present below a description of the structures mapped in the studied  
227 area, highlighting their temporal and spatial relationships with the post-caldera geological formations. We identified two  
228 inactive faults (Maxtaloya and Arroyo Grande), a morphological lineament (Las Papas) and two currently active faults  
229 (Los Humeros and Loma Blanca).

#### 230 **4.1.1 Las Papas lineament (sites LH-07, LH-08)**

231 The E-W trending Las Papas lineament is localised within the Cuicuiltic Member (LH-07; Fig. 5b). We identified an  
232 erosional surface along the scarp, where unaltered and undeformed Cuicuiltic Member rocks rest above the Xoxoctic  
233 Tuff (LH-08, Fig. 5c). The E-W trending morphological lineament of Las Papas is probably due to differential erosion  
234 of the softer layers of the pyroclastic deposits, successively blanketed by the Cuicuiltic Member.

#### 235 4.1.2 Arroyo Grande (site LH-09) and Maxtaloya scarps

236 The NE-SW Arroyo Grande scarp (Fig. 6a) exposes strongly altered and faulted (NW striking faults, mean attitude  
237 N144°/68°, number of data ( $n$ ) = 8) lavas and ignimbrites unconformably covered by the unaltered Cuicuiltic Member  
238 (Fig.6b). The offset observed at the outcrop-scale for the single fault strands is ca. 0.5 m, with a dominant normal dip-  
239 slip kinematics (pitch angle of the slickenlines ranging 99°-106°). The inferred cumulative displacement at Arroyo  
240 Grande is ~ 10 m. Similarly, an outcrop on the Maxtaloya scarp (in front of well H-6) shows altered trachyandesites  
241 covered by unaltered Cuicuiltic Member rocks (Fig. 6c).

#### 242 4.1.3 Los Humeros (site LH-10)

243 The fault scarp of the N-S striking (mean attitude N174°/73°,  $n$ = 8) Los Humeros Fault exposes the altered portions of  
244 the Cuicuiltic Member. Fault population analysis reveals a dominant normal dip-slip (mean pitch angle of the  
245 slickenlines: 84°) kinematics, as documented by both Riedel shears and carbonate-quartz growth steps. The main fault  
246 surface is sutured by a trachyandesitic extrusion (Fig. 6d), localised along an aligned N-S dome (site LH-11 in Fig. 4).  
247 Moreover, ~150 m southward from the outcrop of the fault scarp, a 5 × 3 m wide trachyandesitic plug shows vertical  
248 striation on its surface due to a subsurface vertical flow of the trachyandesite (Fig. 6e). The observed displacement at  
249 the outcrop scale, as indicated by the height of the fault scarp, is ~ 10 m.

#### 250 4.1.4 Loma Blanca (LH-01, LH-02)

251 The Loma Blanca Fault system (sites LH-01 and LH-02) is located in an active degassing area, where faults and  
252 fractures are frequent. The fault system is on top of an elongated crest (within an apical depression) of a morphological  
253 bulge, ~ 1 km in width and 30 m in height. At this location, the Cuicuiltic Member and the underlying trachyandesite  
254 lavas are strongly altered (Fig. 6f). Evidence of stockwork veining and diffuse fracturing of the lavas suggests  
255 hydrofracturing and structurally controlled fluid flow and alteration. A set of NNE-SSW striking conjugate extensional  
256 faulting and jointing (joint spacing ~0.5 m) is observed. The faults (mean attitude N26°/71°,  $n$ = 6) show a normal dip-  
257 slip kinematics (pitch of the slickenlines ranging 82°-104°). Joint systems found in the Cuicuiltic Member strike sub-  
258 parallel to the faults (mean attitude N37°/72°,  $n$ = 14). The inferred cumulative displacement of the faults, estimated by  
259 the depth of the apical depression, is ~ 5 m.

260 In summary, the 22 mapped faults in all the structural outcrops of the area show a main NNW-SSE strike (Fig. 6g) with  
261 a dominant dip slip movement (mean pitch angle of slickenlines 88°,  $n$ = 16) which is sub-parallel to the N-S elongation  
262 of the lava domes and the Xalapasco crater.

#### 263 4.2 Experimental results

264 Here we show three representative experiments with increasing overburden thickness (experiments 1-3-5 with  $T$ = 10,  
265 30 and 50 mm). Table 4 shows the measured parameters in the experiments. Some experiments (1-2 and 3-4) were  
266 replicated with the same imposed boundary conditions and show the same result (*i.e. apical depression width and dome*  
267 *diameter*), which ensures model reproducibility (Fig. 8 and Fig. S1 Fig. 8 and Fig. S1).

268 Overall, the experiments show a similar deformation pattern: a first stage characterized by the uplift of a sub-circular  
269 dome, bordered by inward dipping reverse faults, and a second stage characterized by the subsidence of the apical part  
270 of the dome where normal faulting occurs (apical depression formation Fig. 7a-i). The reverse and normal faults are ring  
271 faults and are associated with the formation of radial fractures from the dome centre. A different shape of the apical



272 depression is observed with  $T/D > 0.12$ . In exp.1 ( $T/D = 0.12$ ) an annular peripheral depression formed as the silicone  
273 reached the surface at the edge of the cylinder (Fig.7c). Conversely, in exp. 3 and 5 ( $T/D= 0.37$  and  $0.63$  respectively) a  
274 sub-circular apical depression formed as the silicone reached the surface at the centre of the dome (Fig.7g, m).  
275 Despite the  $T/D$  ratio, all the experiments show that both the dome diameter and apical depression width increase  
276 linearly with the overburden thickness (ranging from 105 to 164 mm and ~~from~~ 14 to 58 mm respectively, Table 4,  
277 Fig.8). The dome diameter increases abruptly with time, becoming almost constant at an early stage of the experiment  
278 (Fig.9a); the apical depression width shows a similar pattern even if it enlarges slightly with time (after the first abrupt  
279 increase) as the silicone rises towards the surface (Fig. 9b), suggesting that the intrusion depth has a higher influence  
280 on the apical depression width, in agreement with Brothelande and Merle (2015).

281

## 282 5. Discussion

### 283 5.1 Interpretation of the analogue experiments

284 The deformation pattern observed in the analogue experiments for thicker overburdens (experiments 3-4 and 5 with  
285  $T/D= 0.37$  and  $0.63$ ), showing a sub-circular dome and an apical depression, is in agreement with previous analogue  
286 experimental results (Acocella et al., 2001; Marti et al. 1994; Walter and Troll 2001). However, for thinner overburdens  
287 (exps. 1-2,  $T/D= 0.12$ ), we observed a new deformation pattern at the surface consisting of an annular peripheral  
288 depression due to the rising of the silicone at the edge of the cylinder rather than its centre. We infer that in these  
289 experiments, since the rising silicone was very close to the surface, the sagging of the sand overburden pushed  
290 downward the centre of the silicone that squeezed up at the edges of the cylinder. Such process may also explain the  
291 two linear grabens that formed in the experiments with elliptical sources for small overburden thicknesses (ratio  $T/D \sim$   
292  $0.1$ , Brothelande and Merle 2015).

293 The deformation pattern observed in our experiments is independent ~~with respect to~~ the imposed strain (i.e. uplift)  
294 rate or the viscosity of the intruding material as suggested by the similarity with results obtained in previous studies  
295 with higher strain rates (Acocella and Mulugeta, 2002) or lower viscosity intruding materials (Galetto et al., 2017; Marti  
296 et al. 1994; Walter and Troll, 2001). On the other hand, the occurrence of an apical depression is dependent on the  
297 thickness (i.e. depth) of the intrusion since thin intrusions relative to their depths will generate sub-circular domes  
298 without any apical depression (Galland et al., 2009; Galland, 2012). Moreover, our results confirm that the apical  
299 depression width shows a linear correlation with the source depth (Fig. 8) as estimated in Brothelande and Merle (2015)  
300 for elongated sources. This evidence documents that such relation is independent ~~from~~ of the source eccentricity or  
301 shape of the extensional structures at the top of the dome (i.e. linear graben or sub-circular depression) suggesting that  
302 any elongation of the surface structure represents only a minor complication of the basic deformation pattern as already  
303 pointed out by (Roche et al., 2000).

304

### 305 5.2 Origin and extent of the resurgence in the LHVC

306 The distribution of ~~the~~ alteration patterns and deformation characteristics of the ~~post-post~~-caldera deposits can be used  
307 to infer the origin and extent of the uplift within the ~~LHVC~~Los Potreros resurgent caldera. ~~In particular, whether the~~The  
308 ~~extent of the local deformation and alteration of the ubiquitous~~ 7.4 ka Cuicuiltic Member, ~~which blankets the caldera~~  
309 ~~floor, was involved~~involved in the deformation and alteration allow constraining the spatio-temporal evolution of the  
310 surficial deformation and associated uplifts in Los Potreros. Unaltered and undeformed deposits of the Cuicuiltic  
311 Member crop out along the E-W Las Papas lineament and unconformably cover altered and faulted lavas and  
312 ignimbrites along the Arroyo Grande and Maxtaloya scarps. Alteration and deformation of the Cuicuiltic Member

313 occurs along the Los Humeros Fault scarp and within the apical depression of the Loma Blanca bulge. The vertical  
314 striations of the trachyandesitic plug near the Los Humeros fault scarp suggest that the ascent of the plug induced the  
315 uplift, the normal dip-slip faulting and alteration of the Cuicuiltic Member.

316 The observations suggest that Los Potreros is not a classic resurgent caldera (i.e. a caldera characterised by a large-scale  
317 process localized in a single area) but is characterised by ~~a discontinuous~~ uplift ~~process~~ ~~pulses~~ ~~discontinuous~~ in space  
318 and time, inducing small-scale deformations at each pulse (Fig. 10a-d). In particular, it was active in the south and  
319 north-eastern sector of the caldera, at Maxtaloya and Arroyo Grande (Fig. 10a), prior to the deposition of the Cuicuiltic  
320 Member (~ 7.4 ka), and then ~~moved~~ ~~shifted~~ towards N along the Los Humeros and Loma Blanca scarps during and post  
321 the eruption of the Cuicuiltic Member (Fig. 10b-d). The felsic lava found at the Los Humeros Fault scarp shows a  
322 similar mineral assemblage to the felsic domes located further south (Fig. 4); thus, the Los Humeros scarp may  
323 represent the final stage (i.e. effusive eruption of felsic magmas, (Fig. 10c) of the uplift process, which is thus driven by  
324 the ascent of relatively narrow (hundreds of meters) and highly viscous felsic magma batches. This is supported by the  
325 N-S elongation of the identified lava domes which is sub-parallel to the orientation of the measured fault planes (NNW-  
326 SSE), indicating that the observed deformation is closely related to the post-caldera volcanism. The ~~ascent~~ ~~emplacement~~  
327 of such magma bodies is inferred here to drive the recent uplift and deformation of the Loma Blanca bulge, as suggested  
328 by the active fumaroles and extensive alteration of both the Cuicuiltic Member and post-caldera lavas (Fig. 10d). The  
329 ~~presence of such~~ ~~recent emplacement of~~ shallow magma bodies ~~is also suggested by~~ ~~should be considered as a possible~~  
330 ~~scenario for the interpretation of~~ the ~~four major earthquakes recorded~~ ~~seismicity~~ in Los Potreros, which have been  
331 ~~previously so far~~ interpreted ~~to be~~ ~~as~~ induced by geothermal exploitation (Lermo et al., 2018). ~~However, since~~ ~~In facts,~~  
332 ~~the magnitude of the seismic events induced by geothermal exploitation activities is usually lower (i.e. < 3, Evans et al.,~~  
333 ~~2012 and references therein),~~ the ~~higher~~ ~~highest~~ magnitude ~~of the recent seismicity reached~~ (between 3.2 and 4.2) ~~of the~~  
334 ~~earthquakes in Los Potreros suggests that they~~ ~~and~~ may ~~well~~ be ~~more likely of~~ ~~consistent with a~~ volcano-tectonic origin  
335 due to shallow magma emplacement, ~~more than induced by reinjection of hydrothermal fluids (cf. Evans et al., 2012~~  
336 ~~and references therein).~~

337 To further support the above interpretation from field observations, results from the presented analogue models were  
338 used to constrain the magma source depth from the geometrical parameters measured in the experiments ( $L_g$ ,  $\theta$ ,  $\alpha$ , Table  
339 4). We calculated the theoretical overburden thickness (i.e. the intrusion depth,  $T_t$ , Table 4) as follow (Brothelande and  
340 Merle, 2015):

$$341 \quad T_t = \frac{1}{2} L_g \times \frac{\sin(\theta + \alpha)}{\cos \theta} \quad (1)$$

342 Comparing the percentage difference ( $\sigma$ ) between the imposed experimental (T) and theoretical ( $T_t$ ) overburden  
343 thickness values, we calculate the associated error in the evaluation of the intrusion depth in the models ( $\sigma$ , Table 4,  
344 Fig. 8). We then use equation (1) for the evaluation of the heat source depth at the Loma Blanca bulge considering  $\sigma \sim$   
345 40 % (maximum value of the experiments excluding those showing an annular depression that was not observed in the  
346 field). For the Loma Blanca bulge  $L_g = 286$  m,  $\theta = 71^\circ$ ,  $\alpha = 4.5^\circ$ , the estimated intrusion depth is  $425 \pm 170$  m. Such  
347 relatively shallow depth is within the range of depths of rhyolitic-dacitic ~~domes~~ ~~bodies~~ drilled in geothermal wells  
348 (spanning from ~~-300~~ to ~~-1700~~ m, Fig. 2a-b) and is consistent with the hypothesis that the uplift is driven by small and  
349 delocalized magmatic intrusions, as suggested by the field data.

350 These rhyolites-dacites ~~bodies~~ have been previously interpreted ~~of as~~ subaerial ~~in~~ origin (Carrasco-Núñez et al., 2017a),  
351 but we suggest that at least some of them can be reinterpreted as intrusions of felsic cryptodomes based on the  
352 following considerations: (i) the occurrence of rhyolite-dacite lava bodies within the thick pre-caldera old andesite  
353 sequence is unusual and does not have a subaerial counterpart; (ii) the rhyolite body in well H-20 (Fig. 2b) up warps

354 both the intracaldera ignimbrite sequence and the post-caldera lavas (showing a reduced thickness) indicating that the  
355 caldera forming ignimbrites do not levelled out the paleo-topography, as it should be expected; and (iii) the top of the  
356 Xaltipan ignimbrite shows ~~an~~ higher depth variation than the pre caldera andesite (Fig. 2a) highlighting a local and  
357 discontinuous uplifting of the Xaltipan ignimbrite. Such evidence can be more easily reconciled with the intrusion of  
358 felsic cryptodomes within the volcanic sequence, ~~rather than with a regular layer cake stratigraphy~~.

359

### 360 5.3 Implications for the structure of the LHVC geothermal field

361 The combination of field and modelling data support that the uplift in Los Potreros caldera is due to multiple  
362 deformation sources in narrow areas that do not represent resurgence *sensu stricto*. Such localized recent deformation  
363 within Los Potreros caldera appears to be linked to small magmatic intrusions located at relatively shallow depths (i.e. <  
364 1 km) as in Loma Blanca, where the estimated intrusion depth calculated from the experimental data is  $425 \pm 170$  m.

365 This model differs from the generally accepted idea of a resurgence in Los Potreros induced by the inflation of a saucer  
366 or cup shaped deep magmatic intrusion (Norini et al., 2015, 2019), which may be active at a larger scale but does not  
367 explain the highly discontinuous deformation and alteration patterns with pulses scattered along the caldera floor. The  
368 resurgence is inferred to be centred beneath the sector of the caldera traversed by the E-W lineaments and limited by the  
369 Maxtaloya and Arroyo Grande faults (sector S1 in Norini et al., 2015). The Neither the thermal anomalies identified by  
370 Norini et al. (2015) fit well with the classic resurgence as show that the temperatures are unexpectedly cold beneath the  
371 ~~inferred~~ centre of the inferred resurgent block, where the highest temperatures should be expected. By contrast, sharp  
372 and narrow temperature peaks, spatially coincident with Los Humeros and Loma Blanca faults, are consistent with the  
373 presence of shallow and delocalized heat sources. Indeed, the inflation of the deep magma chamber of the LHVC,  
374 inferred to be at 5 to 7-8 km of depth (Verma, 1983, 2000, 2011) and extending 9 km in radius and 6 km in length (thus  
375 coinciding with the Los Humeros caldera rim, Verma et al., 1990), should have ~~resulted in~~ induced a much wider uplift  
376 and with higher magnitude than the one observed in the field. Resurgence resulting from magma remobilization of the  
377 deep chamber that produced collapse is characterized by a larger-scale surface deformation (thousands of meters of  
378 uplift extending for tens of kilometres on the surface) as shown in many large calderas worldwide (Toba, de Silva et  
379 al., 2015; Cerro Galan, Folkes et al., 2011; Ischia, Carlino, 2012, Selva et al. 2019).

380 It is therefore unlikely that the replenishment of new magma in the caldera forming deep magma chamber accounts for  
381 the magnitude (few tens of meters) and discontinuous spatial distribution of the deformation in Los Potreros.

382 Such a model of the recent uplifting in Los Potreros is supported by field-based petrographic-mineralogical analysis  
383 showing that the present-day magmatic plumbing system is characterized by multiple magma levels spanning from a  
384 deep (30-33 km) basaltic reservoir to very shallow (~ 1.5 km), smaller, trachyandesitic-trachytic magma batches (Lucci  
385 et al., under review2020).

386 A similar model of the plumbing system has been proposed to explain the eruptive activity of Usu volcano (Japan) since  
387 1663, a post caldera cone of the Toya caldera consisting of a basaltic main edifice surmounted by ~~3~~ three felsic lava  
388 domes and more than ~~10~~ ten cryptodomes. Petrochemical data at Usu suggest the presence of multiple magma batches  
389 (i.e. sills) at 0.25-2 km deep that originated from partial melting of a metagabbro (Matsumoto and Nakagawa, 2010;  
390 Tomya et al., 2010).

391 Our proposed model has implications for planning future geothermal exploration: siting of future geothermal wells  
392 should consider that the presence of shallow heat sources within the caldera ~~may~~ might complicate the pattern of  
393 isotherms associated with the deeper heat flow.

## 394 **6 Conclusions**

395 By integrating field work with analogue models, we constrain the ~~late-Late~~ Pleistocene-Holocene spatio-temporal  
396 evolution of volcanism of the LHVC and estimate the depth of the magmatic intrusions feeding the active geothermal  
397 system. New findings on experimental analogue models of resurgent domes are also provided.

398 These are the main results that can be extracted from this study:

399 1. The distribution of the alteration patterns and deformation of the Cuicuiltic Member suggests that the recent (post-  
400 caldera collapse) uplift in Los Potreros caldera moved progressively northwards, from the south and north-eastern  
401 sector of the caldera towards N along the Los Humeros and Loma Blanca scarps.

402 2. The estimated depth of the intrusions responsible for such uplift is very shallow, as calculated from the experimental  
403 data for the Loma Blanca bulge ( $425 \pm 170$  m).

404 3. The recent uplift in Los Potreros is discontinuous in space and time, inducing small-scale (areal extent  $\sim 1$  km<sup>2</sup>)  
405 deformations originating from multiple and shallow ( $< 1$  km depth) magmatic bodies, thus not representing a classic  
406 resurgent caldera, which usually involves ~~large-scale~~ large-scale deformation (areal extent of several km<sup>2</sup>).

407 4. The relation ~~ship between the depth of the~~ between the depth of the magmatic source and the surface parameters of  
408 resurgent domes is independent ~~from-of~~ the source eccentricity, similarly to what already verified for sub-circular  
409 intrusions.

410

## 411 **Acknowledgements**

412 CFE is kindly acknowledged for allowing work on the Los Humeros geothermal field. Federico Galetto helped for laser  
413 scanner data processing. Fabio Corbi and Matteo Trolese provided technical support in building the experimental set-up.  
414 Gianluca Norini is acknowledged for logistic support in the field. Alessandra Pensa kindly helped with figure drawings.  
415 Funded by the European Union's Horizon 2020 GEMex Project (grant agreement No. 727550) and by the Mexican  
416 Energy Sustainability Fund CONACYT-SENER, WP 4.5 of the Project 2015-04-268074. More information can be  
417 found on the GEMex Website: <http://www.gemex-h2020.eu>. The Grant to Department of Science, Roma Tre University  
418 (MIUR-Italy Dipartimenti di Eccellenza, ARTICOLO 1, COMMI 314 – 337 LEGGE 232/2016) is gratefully  
419 acknowledged.

420

## 421 **References**

422 Acocella, V.: Great challenges in volcanology: how does the volcano factory work?, *Front. Earth Sci.*, 2:4,  
423 <https://doi.org/10.3389/feart.2014.00004>, 2014.

424 Acocella, V., and Funicello, R.: The interaction between regional and local tectonics during resurgent doming: the case  
425 of the island of Ischia, Italy, *J. Volcanol. Geoth. Res.*, 88, 109-123, [https://doi.org/10.1016/S0377-0273\(98\)00109-7](https://doi.org/10.1016/S0377-0273(98)00109-7),  
426 1999.

427 Acocella, V., and Mulugeta, G.: Experiments simulating surface deformation induced by pluton emplacement,  
428 *Tectonophysics*, 352, 275-293, [https://doi.org/10.1016/S0040-1951\(02\)00218-4](https://doi.org/10.1016/S0040-1951(02)00218-4), 2002.

429 Acocella, V., Cifelli, F., and Funicello, R.: The control of overburden thickness on resurgent domes, *J. Volcanol. Geoth.*  
430 *Res.*, 111, 137–153, [https://doi.org/10.1016/S0377-0273\(01\)00224-4](https://doi.org/10.1016/S0377-0273(01)00224-4), 2001.

431 Arellano, V.M., García, A., Barragán, R.M., Izquierdo, G., Aragón, A., and Nieva, D.: An updated conceptual model of  
432 the Los Humeros geothermal reservoir (Mexico), *J. Volcanol. Geoth. Res.*, 124, 67–88, [https://doi.org/10.1016/S0377-0273\(03\)00045-3](https://doi.org/10.1016/S0377-0273(03)00045-3), 2003.

433

434 Beavon, R.V.: A resurgent cauldron in the early Paleozoic of Wales, U.K., *J. Volcanol. Geoth. Res.*, 7, 157-174,  
435 [https://doi.org/10.1016/0377-0273\(80\)90025-6](https://doi.org/10.1016/0377-0273(80)90025-6), 1980.

436 Brothelande, E., Peltier, A., Got, J.L., Merle, O., Lardy, M., and Garaebiti, E.: Constraints on the source of resurgent  
437 doming inferred from analogue and numerical modeling — Implications on the current feeding system of the Yenkahe  
438 dome–Yasur volcano complex (Vanuatu), *J. Volcanol. Geoth. Res.*, 322, 225–240,  
439 <https://doi.org/10.1016/j.jvolgeores.2015.11.023>, 2016.

440 Brothelande, E., and Merle, O.: Estimation of magma depth for resurgent domes: An experimental approach, *Earth  
441 Planet. Sc. Lett.*, 412, 143–151, <https://doi.org/10.1016/j.epsl.2014.12.011>, 2015.

442 Calcagno, P., Evanno, G., Trumpy, E., Carlos Gutiérrez-Negrín, L., MacIás, J.L., Carrasco-Núñez, G., and Liotta, D.:  
443 Preliminary 3-D geological models of Los Humeros and Acoculco geothermal fields (Mexico)-H2020 GEMex Project,  
444 *Adv. Geosci.*, 45, 321–333, <https://doi.org/10.5194/adgeo-45-321-2018>, 2018.

445 Carlino, S.: The process of resurgence for Ischia Island (southern Italy) since 55 ka: The laccolith model and  
446 implications for eruption forecasting, *B. Volcanol.*, 74, 947–961. <https://doi.org/10.1007/s00445-012-0578-0>, 2012.

447 Carrasco-Núñez, G., and Branney, M.J.: Progressive assembly of a massive layer of ignimbrite with a normal-to-reverse  
448 compositional zoning: The Zaragoza ignimbrite of central Mexico, *B. Volcanol.*, 68, 3–20,  
449 <https://doi.org/10.1007/s00445-005-0416-8>, 2005.

450 Carrasco-Núñez, G., McCurry, M., Branney, M.J., Norry, M., and Willcox, C.: Complex magma mixing, mingling, and  
451 withdrawal associated with an intra-Plinian ignimbrite eruption at a large silicic caldera volcano: Los Humeros of  
452 central Mexico, *Bull. Geol. Soc. Am.*, 124, 1793–1809, <https://doi.org/10.1130/B30501.1>, 2012.

453 Carrasco-Núñez, G., López-Martínez, M., Hernández, J., and Vargas, V.: Subsurface stratigraphy and its correlation  
454 with the surficial geology at Los Humeros geothermal field, eastern Trans-Mexican Volcanic Belt, *Geothermics*, 67, 1–  
455 17, <https://doi.org/10.1016/j.geothermics.2017.01.001>, 2017a.

456 Carrasco-Núñez, G., Hernández, J., De León, L., Dávila, P., Norini, G., Bernal, J.P., Jicha, B., Navarro, M., López-  
457 Quiroz, P., and Digitalis, T.: Geologic Map of Los Humeros volcanic complex and geothermal field, eastern Trans-  
458 Mexican Volcanic Belt, *Terra Digitalis*, 1, 1–11, <https://doi.org/10.22201/igg.terradigitalis.2017.2.24.78>, 2017b.

459 Carrasco-Núñez, G., Bernal, J.P., Dávila, P., Jicha, B., Giordano, G., and Hernández, J.: Reappraisal of Los Humeros  
460 volcanic complex by new U/Th zircon and <sup>40</sup>Ar/<sup>39</sup>Ar dating: Implications for greater geothermal potential, *Geochem.  
461 Geophys. Geosy.*, 19, 132-149, <https://doi.org/10.1002/2017GC007044>, 2018.

462 [Cashman, K. V., & Giordano, G.: Calderas and magma reservoirs-, \*J. Volcanol. Geoth. Res. Journal of Volcanology  
463 and Geothermal Research\*, 288, 28-45, <https://doi.org/10.1016/j.jvolgeores.2014.09.007>, 2014.](https://doi.org/10.1016/j.jvolgeores.2014.09.007)

464 Catalano, S., De Guidi, G., Lanzafame, G., Monaco, C., and Tortotici, L.: Late quaternary deformation on the island on  
465 Pantelleria: new constraints for the recent tectonic evolution of the Sicily Channel Rift (southern Italy). *J. Geodyn.* 48,  
466 75–82, 2009.

467 Chang, W.L., Smith, R.B., Wicks, C., Farrell, J.M., and Puskas, C.M.: Accelerated uplift and magmatic intrusion of the  
468 Yellowstone Caldera, 2004 to 2006, *Science*, 318, 952-956, <https://doi.org/10.1126/science.1146842>, 2007.

469 Christiansen, R.L., Lipman, P.W., Carr, W.J., Byers, F.M., Orkild, P.P., and Sargent, K.A.: Timber Mountain-Oasis  
470 Valley caldera complex of southern Nevada, *Geol. Soc. Am. Bull.*, 88, 943-959, [https://doi.org/10.1130/0016-  
471 7606\(1977\)88<943:TMVCCO>2.0.CO;2](https://doi.org/10.1130/0016-7606(1977)88<943:TMVCCO>2.0.CO;2), 1977.

472 Dávila-Harris, P., and Carrasco-Núñez, G.: An unusual syn-eruptive bimodal eruption: The Holocene Cuicuiltic  
473 Member at Los Humeros caldera, Mexico, *J. Volcanol. Geoth. Res.*, 271, 24–42,  
474 <https://doi.org/10.1016/j.jvolgeores.2013.11.020>, 2014.

475 de Silva, S.L., Mucek, A.E., Gregg, P.M., and Pratomo, I.: Resurgent Toba - field, chronologic, and model constraints  
476 on time scales and mechanisms of resurgence at large calderas, *Front. Earth Sci.*, 3, 1–17,  
477 <https://doi.org/10.3389/feart.2015.00025>, 2015.

478 Doblas, M.: Slickenside kinematic indicators, *Tectonophysics*, 295, 187–197, <https://doi.org/10.1016/S0040->  
479 [1951\(98\)00120-6](https://doi.org/10.1016/S0040-1951(98)00120-6), 1998.

480 Du Bray, E.A., and Pallister, J.S.: Recrystallization and anatexis along the plutonic–volcanic contact of the Turkey  
481 Creek caldera, Arizona, *Geol. Soc. Am. Bull.*, 111, 143–153, <https://doi.org/10.1130/0016->  
482 [7606\(1999\)111<0143:RAAATP>2.3.CO;2](https://doi.org/10.1130/0016-7606(1999)111<0143:RAAATP>2.3.CO;2), 1999.

483 Elston, W.: Mid-Tertiary ash flow tuff cauldrons, southwestern New Mexico, *J. Geophys. Res.*, 89, 8733–8750,  
484 <https://doi.org/10.1029/JB089iB10p08733>, 1984.

485 Evans, K.F., Zappone, A., Kraft, T., Deichmann, N., and Moia, F.: A survey of the induced seismic responses to fluid  
486 injection in geothermal and CO<sub>2</sub> reservoirs in Europe, *Geothermics*, 41, 30–54,  
487 <https://doi.org/10.1016/j.geothermics.2011.08.002>, 2012.

488 Ferrari, L., Orozco-Esquivel, T., Manea, V., and Manea, M.: The dynamic history of the Trans-Mexican Volcanic Belt  
489 and the Mexico subduction zone, *Tectonophysics*, 522–523, 122–149, <https://doi.org/10.1016/j.tecto.2011.09.018>, 2012.

490 Ferriz, H., and Mahood, G.A.: Eruption Rates and Compositional Trends at Los Humeros Volcanic Center, Puebla,  
491 Mexico, *J. Geophys. Res.*, 89, 8511–8524, <https://doi.org/10.1029/JB089iB10p08511>, 1984.

492 Folkes, C.B., Wright, H.M., R.A.F. Cas, de Silva, S.L., Lesti, C., and Viramonte, J.G.: A re-appraisal of the stratigraphy  
493 and volcanology of the Cerro Galán volcanic system, NW Argentina, *B. Volcanol.*, 73, 1427–1454,  
494 <https://doi.org/10.1007/s00445-011-0459-y>, 2011.

495 Fridrich, C.J., Smith, R.P., DeWitt, E., McKee, E.H.: Structural, eruptive, and intrusive evolution of the Grizzly Peak  
496 caldera, Sawatch Range, Colorado, *Geol. Soc. Am. Bull.*, 103, 1160–1177, <https://doi.org/10.1130/0016->  
497 [7606\(1991\)103<1160:SEAIEO>2.3.CO;2](https://doi.org/10.1130/0016-7606(1991)103<1160:SEAIEO>2.3.CO;2), 1991.

498 Galetto, F., Acocella, V., and Caricchi, L.: Caldera resurgence driven by magma viscosity contrasts, *Nat. Commun.*, 8,  
499 1–11, <https://doi.org/10.1038/s41467-017-01632-y>, 2017.

500 Galetto, F., Bagnardi, M., Acocella, V., and Hooper, A.: Nonruptive unrest at the caldera of Alcedo Volcano (Galápagos  
501 Islands) revealed by InSAR data and geodetic modelling, *J. Geophys. Res.*, 124, 3365–3381,  
502 <https://doi.org/10.1029/2018JB017103>, 2019.

503 Galland, O.: Experimental modelling of ground deformation associated with shallow magma intrusions, *Earth Planet.*  
504 *Sc. Lett.*, 317–318, 145–156, <https://doi.org/10.1016/j.epsl.2011.10.017>, 2012.

505 Galland, O., Planke, S., Ragnhild Neumann, E., and Malthe-Sørenssen, A.: Experimental modelling of shallow magma  
506 emplacement: Application to saucer-shaped intrusions, *Earth Planet. Sc. Lett.*, 277, 373–383,  
507 <https://doi.org/10.1016/j.epsl.2008.11.003>, 2009.

508 [Giordano, G., Pinton, A., Cianfarra, P., Baez, W., Chiodi, A., Viramonte, J., Norini G., and Groppelli, G.: Structural](https://doi.org/10.1016/j.jvolgeores.2012.09.009)  
509 [control on geothermal circulation in the Cerro Tuzgle–Tocomar geothermal volcanic area \(Puna plateau, Argentina\).; J.](https://doi.org/10.1016/j.jvolgeores.2012.09.009)  
510 [Volcanol. Geotherm. Res., 249, 77–94. <https://doi.org/10.1016/j.jvolgeores.2012.09.009>, 2013.](https://doi.org/10.1016/j.jvolgeores.2012.09.009)

511 [Giordano, G., De Benedetti, A. A., Bonamico, A., Ramazzotti, P., and Mattei, M.: Incorporating surface indicators of](https://doi.org/10.1016/j.earscirev.2013.10.010)  
512 [reservoir permeability into reservoir volume calculations: Application to the Colli Albani caldera and the Central Italy](https://doi.org/10.1016/j.earscirev.2013.10.010)  
513 [Geothermal Province. Earth-Sci. enee Rev. iews.](https://doi.org/10.1016/j.earscirev.2013.10.010) 128, 75–92, <https://doi.org/10.1016/j.earscirev.2013.10.010>, 2014.

514 Goto, Y., and McPhie, J.: Tectonics, structure, and resurgence of the largest Quaternary caldera in Japan: Kutcharo,  
515 Hokkaido, *Geol. Soc. Am. Bull.*, 130, 1307–1322, <https://doi.org/10.1130/B31900.1>, 2018.

516 Guillou-Frotier, L., Burov, E.B., and Milési, J.P.: Genetic links between ash-flow calderas and associated ore deposits  
517 as revealed by large-scale thermo-mechanical modelling, *J. Volcanol. Geoth. Res.*, 102, 339–361,  
518 [https://doi.org/10.1016/S0377-0273\(00\)00246-8](https://doi.org/10.1016/S0377-0273(00)00246-8), 2000.

519 Hildreth, W., Fierstein, J., and Calvert, A.: Early postcaldera rhyolite and structural resurgence at Long Valley  
520 Caldera, California, *J. Volcanol. Geoth. Res.*, 335, 1-34, <http://dx.doi.org/10.1016/j.jvolgeores.2017.01.005>, 2017.

521 Kennedy, B., Wilcock, J., and Stix, J.: Caldera resurgence during magma replenishment and rejuvenation at Valles and  
522 Lake City calderas, *B. Volcanol.*, 74, 1833–1847, <https://doi.org/10.1007/s00445-012-0641-x>, 2012.

523 Lipman, P. W.: The roots of ash flow calderas in Western North America: windows into the tops of granitic batholiths, *J.*  
524 *Geophys. Res.*, 89, 8801–8841, <https://doi.org/10.1029/JB089iB10p08801>, 1984.

525 Lermo, J., Lorenzo, C., Jiménez, N., Ramos, E., Ângulo, J., Israel, J., Téllez, N., Machado, O., Álvarez, I., Torres, R.,  
526 Alfaro R.: Analisis de la actividad sismica (1994-2016), su relacion con los pozos inyectores y productores y aplicación  
527 de nuevas tecnicas geofisica para caracterizar las zonas anómalas del campo geotérmico de Los Humeros, CEMIE-  
528 GEO, Mexico, Internal Rep., 42 pp., 2018.

529 Lucci, F., Carrasco-Núñez, G., Rossetti, F., Theye, T., White, J. C., Urbani, S., Azizi, H., Asahara, Y., and Giordano, G.:  
530 Anatomy of the magmatic plumbing system of Los Humeros Caldera (Mexico): implications for geothermal systems,  
531 *Solid Earth Discuss.*, <https://doi.org/10.5194/se-2019-86>, [in review, 20192020](https://doi.org/10.5194/se-2019-86).

532 Marsh, B.D.: On the mechanics of caldera resurgence, *J. Geophys. Res.*, 89, 8245–8251,  
533 <https://doi.org/10.1029/JB089iB10p08245>, 1984.

534 Martí, J., Ablay, G.J., Redshaw, L.T., and Sparks, R.S.J.: Experimental studies of collapse calderas, *J. Geol. Soc.*  
535 *London*, 151, 919-929, <https://doi.org/10.1144/gsjgs.151.6.0919>, 1994.

536 Merle, O., Borgia, A.: Scaled experiments of volcanic spreading, *J. Geophys. Res.*, 101, 13805-13817,  
537 <https://doi.org/10.1029/95JB03736>, 1996.

538 Morán-Zenteno, D.J., Alba-Aldave, L.A., Solé, J., and Iriondo, A.: A major resurgent caldera in southern Mexico: the  
539 source of the late Eocene Tilzapotla ignimbrite. *J. Volcanol. Geoth. Res.*, 136, 97–119,  
540 <https://doi.org/10.1016/j.jvolgeores.2004.04.002>, 2004.

541 Moretti, R., Troise, C., Sarno, F., and De Natale, G.: Caldera unrest driven by CO<sub>2</sub> induced drying of the deep  
542 hydrothermal system, *Sci. Rep. UK*, 8, <https://doi.org/10.1038/s41598-018-26610-2>, 2018.

543 Mueller, W.U., Stix, J., Corcoran, P.L., Daigneault, R.: Subaqueous calderas in the Archean Abitibi greenstone belt: An  
544 overview and new ideas, *Ore Geol. Rev.*, 35, 4–46, <https://doi.org/10.1016/j.oregeorev.2008.12.003>, 2009.

545 Norini, G., Groppelli, G., Sulpizio, R., Carrasco-Núñez, G., Dávila-Harris, P., Pellicoli, C., Zucca, F., and De Franco,  
546 R.: Structural analysis and thermal remote sensing of the Los Humeros Volcanic Complex: Implications for volcano  
547 structure and geothermal exploration, *J. Volcanol. Geoth. Res.*, 301, 221–237,  
548 <https://doi.org/10.1016/j.jvolgeores.2015.05.014>, 2015.

549 Norini, G., Carrasco-Núñez, G., Corbo-Camargo, F., Lermo, J., Hernández Rojas, J., Castro, C., Bonini, M., Montanari,  
550 D., Corti, G., Moratti, G., Chavez, G., Ramirez, M., and Cedillo F.: The structural architecture of the Los Humeros  
551 volcanic complex and geothermal field, *J. Volcanol. Geoth. Res.*, 381, 312-329.  
552 <https://doi.org/10.1016/j.jvolgeores.2019.06.010>, 2019.

553 Matsumoto, A., and Nakagawa, M.: Formation and evolution of silicic magma plumbing system: Petrology of the  
554 volcanic rocks of Usu volcano, Hokkaido, Japan, *J. Volcanol. Geoth. Res.*, 196, 185–207,  
555 <https://doi.org/10.1016/j.jvolgeores.2010.07.014>, 2010.

556 Pribnow, D.F.C., Schütze, C., Hurter, S.J., Flechsig, C., Sass, J.H.: Fluid flow in the resurgent dome of Long Valley  
557 Caldera: Implications from thermal data and deep electrical sounding. *J. Volcanol. Geoth. Res.*, 127, 329–345,  
558 [https://doi.org/10.1016/S0377-0273\(03\)00175-6](https://doi.org/10.1016/S0377-0273(03)00175-6), 2003.

559 Roche, O., Druitt, T.H., and Merle, O.: Experimental study of caldera formation, *J. Geophys. Res.*, 105,  
560 <https://doi.org/10.1029/1999JB900298>, 395-416, 2000.

561

562 [Selva, J., Acocella, V., Bisson, M., Caliro, S., Costa, A., Della Seta, M., P. De Martino, S. de Vita, C. Federico,  
563 G. Giordano, S. Martino, and C. Cardaci.: Multiple natural hazards at volcanic islands: a review for the Ischia volcano  
564 \(Italy\).- \*Journal of Applied Volcanology\*, 8\(1\), 5., <https://doi.org/10.1186/s13617-019-0086-4>, 2019.](#)

565 Smith, R. L., and Bailey, R. A.: Resurgent cauldrons, *Geol. Soc. Am. Mem.*, 116, 613–662,  
566 <https://doi.org/10.1130/MEM116>, 1968.

567 Stix, J., Kennedy, B., Hannington, M., Gibson, H., Fiske, R., Mueller, W., Franklin, J.: Caldera-forming processes and  
568 the origin of submarine volcanogenic massive sulfide deposits, *Geology*, 31, 375–378, [https://doi.org/10.1130/0091-  
569 7613\(2003\)031<0375:CFPATO>2.0.CO;2](https://doi.org/10.1130/0091-7613(2003)031<0375:CFPATO>2.0.CO;2), 2003.

570 Swanson, E., and McDowell, F.: Geology and geochronology of the Tomochic caldera, Chihuahua, Mexico, *Geol. Soc.  
571 Am. Bull.*, 96, 1477-1482, [https://doi.org/10.1130/0016-7606\(1985\)96<1477:GAGOTT>2.0.CO;2](https://doi.org/10.1130/0016-7606(1985)96<1477:GAGOTT>2.0.CO;2), 1985.

572 Tomiya, A., Takahashi, E., Furukawa, N., Suzuki, T.: Depth and evolution of a silicic magma chamber: Melting  
573 experiments on a low-K rhyolite from Usu volcano, Japan, *J. Petrol.*, 51, 1333–1354,  
574 <https://doi.org/10.1093/petrology/egg021>, 2010.

575 Ueda, H., Nagai, M., and Tanada, T.: Phreatic eruptions and deformation of Ioto Island (Iwo-jima), Japan, triggered by  
576 deep magma injection, *Earth Planets Space*, 70, <https://doi.org/10.1186/s40623-018-0811-y>, 2018.

577 Verma, M.P., Verma, S.P., and Sanvicente, H.: Temperature field simulation with stratification model of magma  
578 chamber under Los Humeros caldera, Puebla, Mexico, *Geothermics*, 19, 187–197, [https://doi.org/10.1016/0375-  
579 6505\(90\)90015-4](https://doi.org/10.1016/0375-6505(90)90015-4), 1990.

580 Verma, S.P., Gómez-Arias, E., and Andaverde, J.: Thermal sensitivity analysis of emplacement of the magma chamber  
581 in Los Humeros caldera, Puebla, Mexico, *Int. Geol. Rev.*, 53, 905–925, <https://doi.org/10.1080/00206810903234296>,  
582 2011.

583 Verma, S.P.: Magma genesis and chamber processes at Los Humeros caldera, Mexico - Nd and Sr isotope data, *Nature*,  
584 302, 52–55, <https://doi.org/10.1038/302052a0>, 1983.

585 Verma, S.P.: Geochemical evidence for a lithospheric source for magmas from Los Humeros caldera, Puebla, Mexico.  
586 *Chem. Geol.* 164, 35–60, [https://doi.org/10.1016/S0009-2541\(99\)00138-2](https://doi.org/10.1016/S0009-2541(99)00138-2), 2000.

587 [Vignaroli, G., Pinton, A., De Benedetti, A. A., Giordano, G., Rossetti, F., Soligo, M., and Berardi, G.: Structural  
588 compartmentalisation of a geothermal system, the Torre Alfina field \(central Italy\).- \*Tectonophysics\*, 608, 482-498.  
589 <https://doi.org/10.1016/j.tecto.2013.08.040>, 2013.](#)

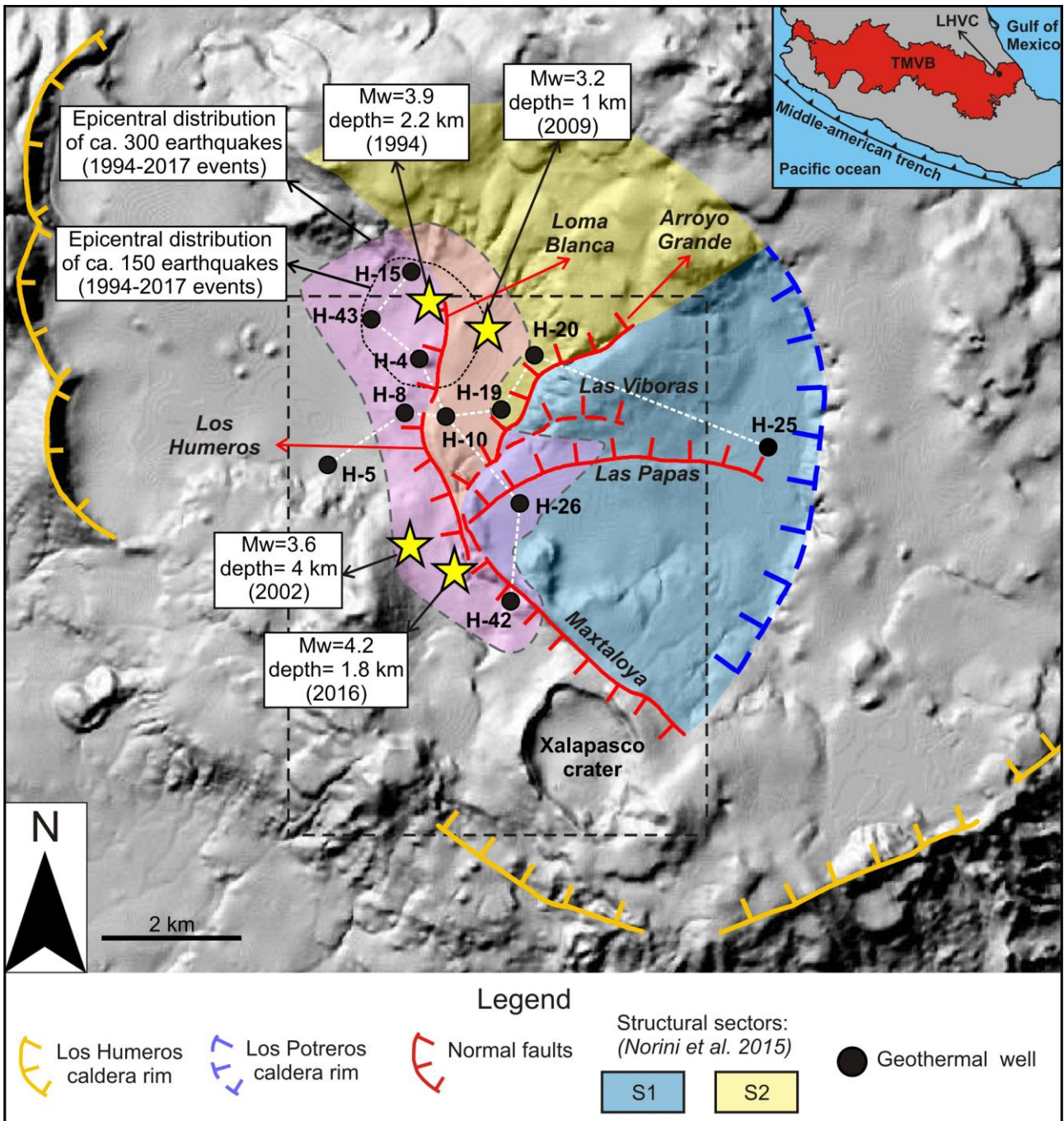
590 [Vignaroli, G., Aldega, L., Balsamo, F., Billi, A., De Benedetti, A. A., De Filippis, L., Giordano G. and Rossetti, F.: A  
591 way to hydrothermal paroxysm, Colli Albani volcano, Italy.- \*Geol. Soc. Am. Bull.\*, 127\(5-6\), 672-687.  
592 <https://doi.org/10.1130/B31139.1>, 2015.](#)

593 Walter, T.R., and Troll, V.R.: Formation of caldera periphery faults: an experimental study, *B. Volcanol.*, 63, 191-203,  
594 <https://doi.org/10.1007/s004450100135>, 2001.

595 Walter, T.R., Wang, R., Acocella, V., Neri, M., Grosser, H., and Zschau, J.: Simultaneous magma and gas eruptions at three  
596 volcanoes in southern Italy: an earthquake trigger ?, *Geology*, 37, 251–254, <https://doi.org/10.1130/G25396A>, 2009.

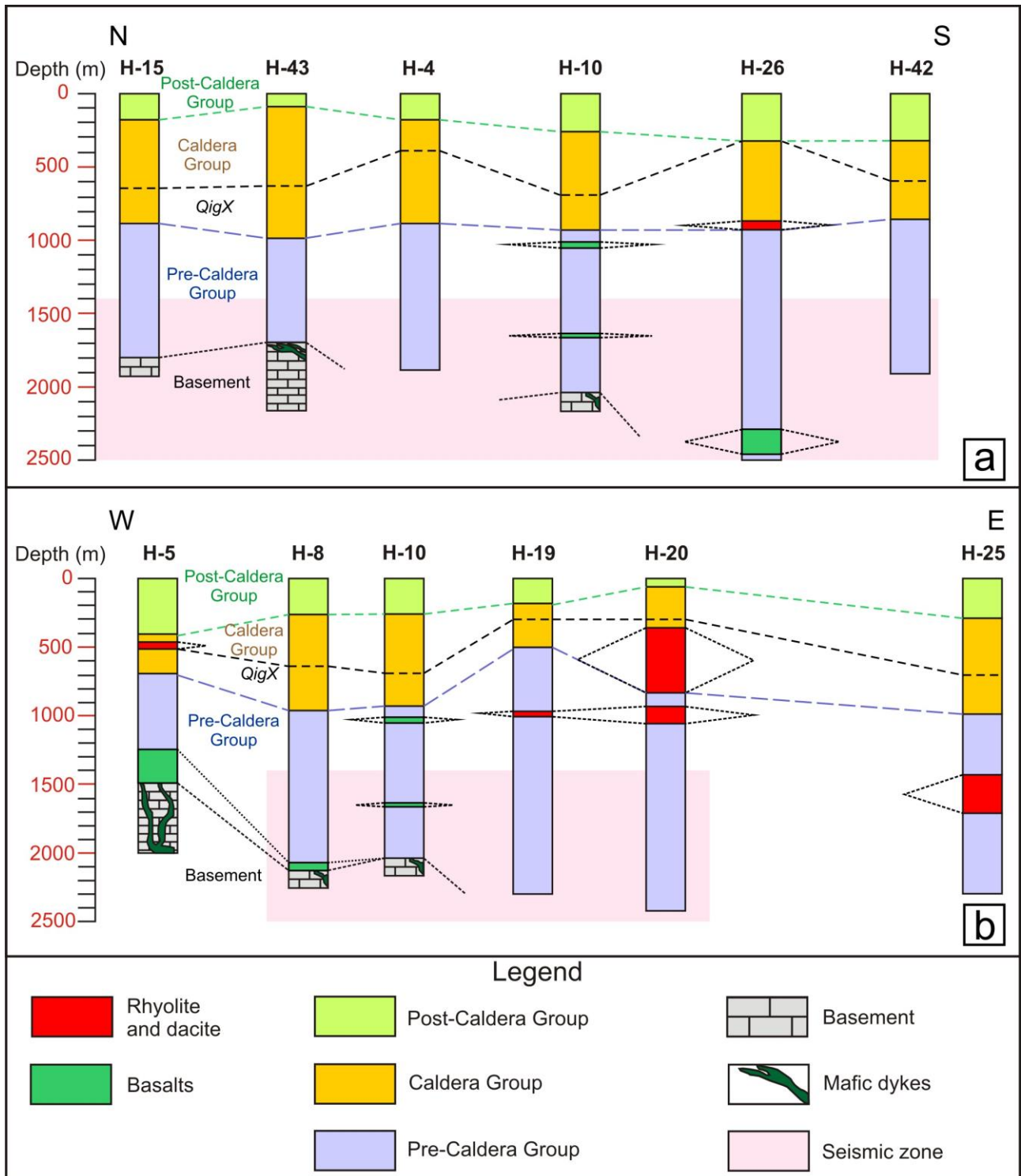


597 Wilcox, C.P.: Eruptive, magmatic and structural evolution of a large explosive caldera volcano, Los Humeros, Central  
598 Mexico, Ph.D. thesis, Department of Geology, University of Leicester, United Kingdom, 317 pp., 2011.



599  
 600 **Figure 1:** Shaded relief image (illuminated from the NE) obtained from 15 m resolution DEM of the Los Humeros Volcanic  
 601 Complex (LHVC) showing the main structural features (faults and caldera rim, modified from Norini et al. (2015); Calcagno  
 602 et al. (2018) and some geothermal wells referred in the text and in Figures 2a-b. The white dashed lines indicate the direction  
 603 of the correlation sections shown in Figures 2a-b. The black rectangle indicates the studied area within the Los Potreros  
 604 Caldera shown in Figure 4. The Inset box show the location of the LHVC (black dot and arrow) within the eastern sector of  
 605 the Trans Mexican Volcanic Belt (TMVB). The structural sectors S1 and S2 correspond to the resurgent block inferred by  
 606 Norini et al. (2015). Seismicity data from Lermo et al. (2018).

607  
 608  
 609  
 610  
 611



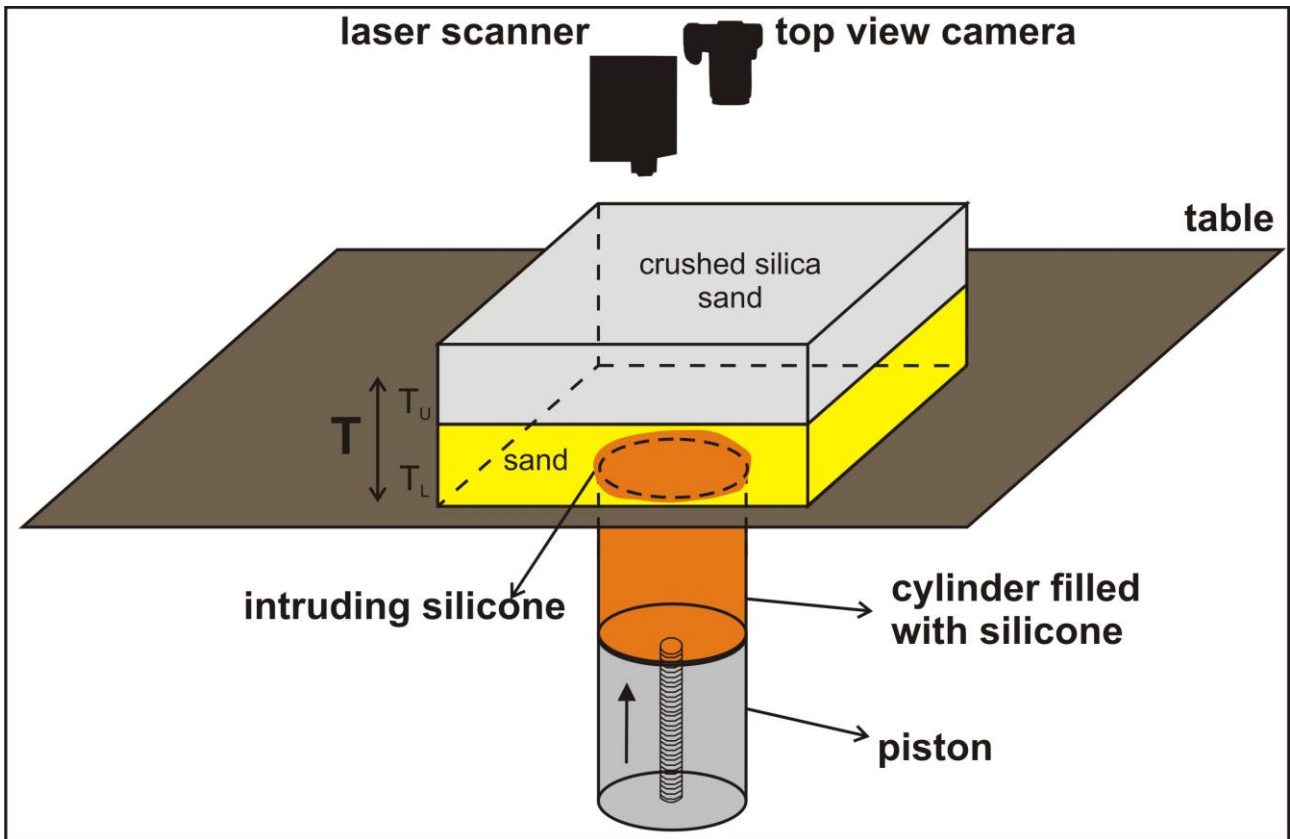
612

613

614

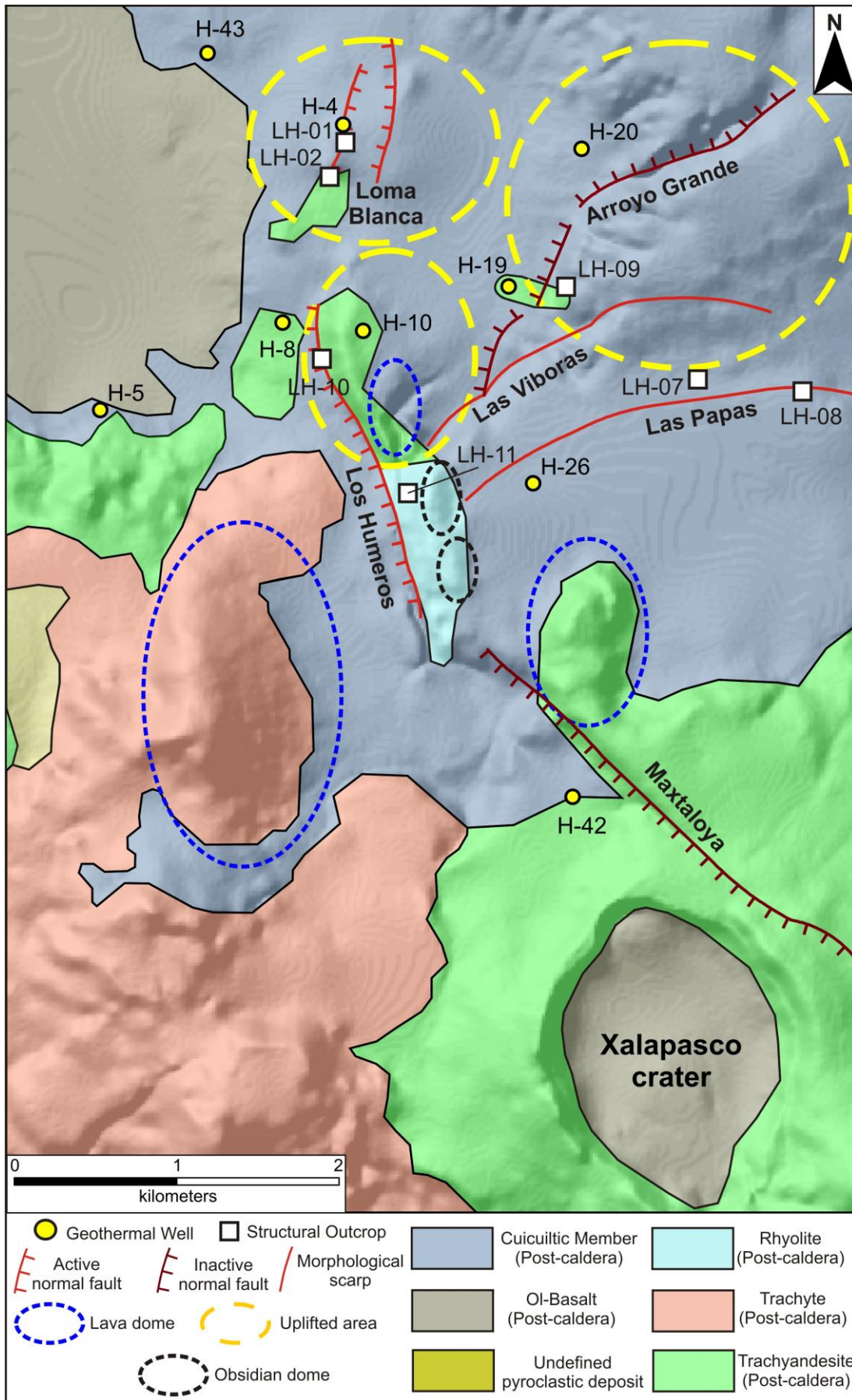
615

Figure 2: In depth correlation of lithostratigraphic units along the N-S (a) and W-E (b) direction (redrawn after Carrasco-Núñez et al. (2017a) and Arellano et al. (2003). Depth:horizontal distance=1:1. Location of the correlation line is shown in Figure 1. QigX= Xaltipan ignimbrite.



616  
 617  
 618  
 619  
 620  
 621  
 622  
 623  
 624  
 625  
 626  
 627  
 628  
 629  
 630  
 631  
 632  
 633  
 634  
 635  
 636  
 637  
 638  
 639

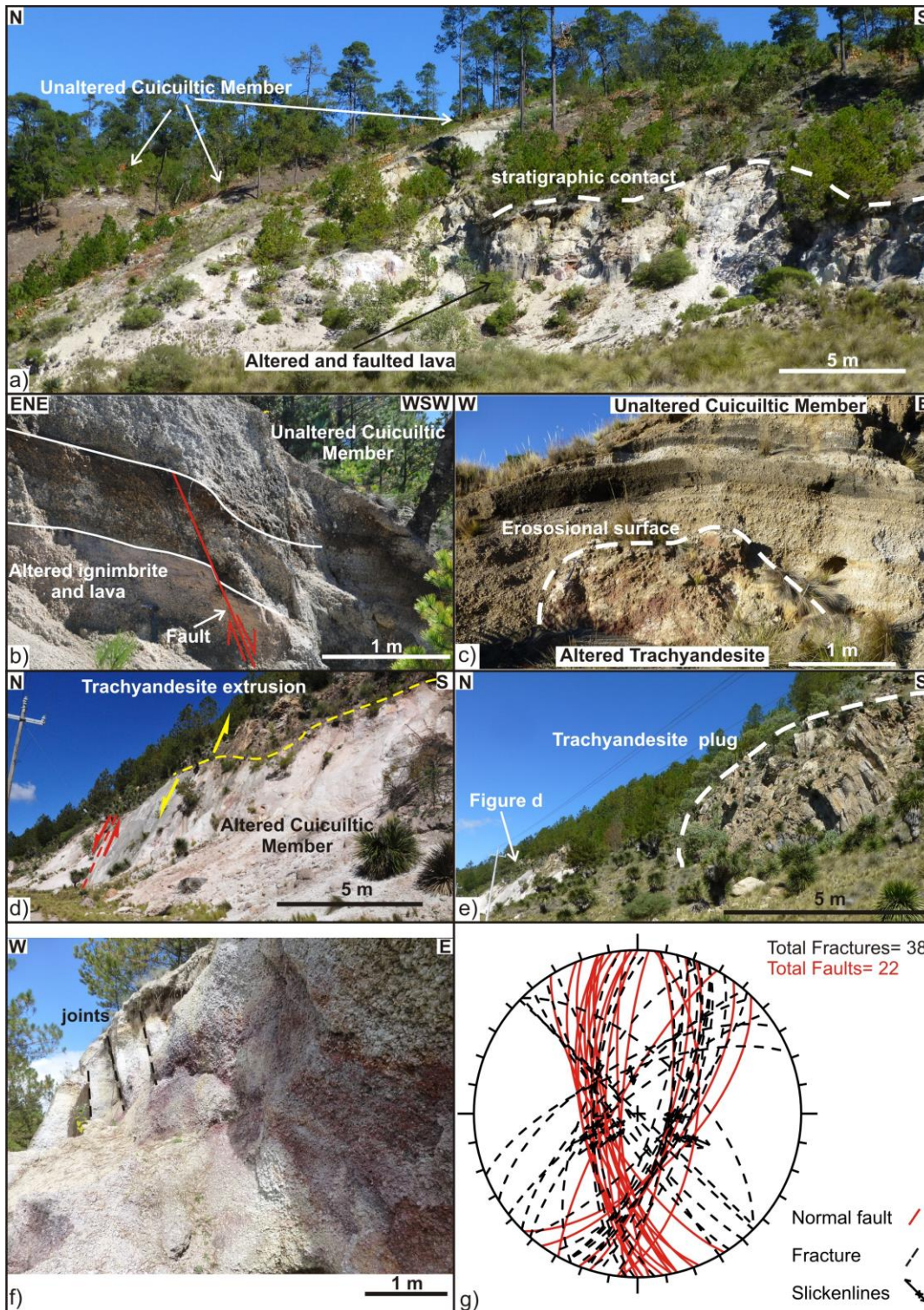
Figure 3: Experimental set-up. A motor controlled piston pushes upward the silicone at a fixed rate (2mm/hr) from the base of the layered sand pack (the diameter of the silicone is 8 cm). A laser scanner and a camera record the surface deformation induced by the intruding silicone.  $T$ = total overburden thickness.  $T_U$ = upper layer thickness,  $T_L$ = lower layer thickness.



640  
641 **Figure 4: Simplified geological structural map of the studied area;reinterpreted after (Norini et al., 2015; Carrasco- Núñez et**  
642 **al., 2017b; Calcagno et al., 2018).**



643  
 644 **Figure 5: a) Panoramic view from Xalapasco crater (looking towards N) of the lava domes aligned N-S. b) Unaltered**  
 645 **Cuicuiltic Member (LH-07). c) Unaltered Cuicuiltic Member covering a layered pyroclastic deposit, which can be laterally**  
 646 **correlated with the Xoxoctic Tuff (LH-08). The erosional surface preceding the deposition of the Cuicuiltic Member is shown**  
 647 **(dashed white line).**



648

649

650

651

652

653

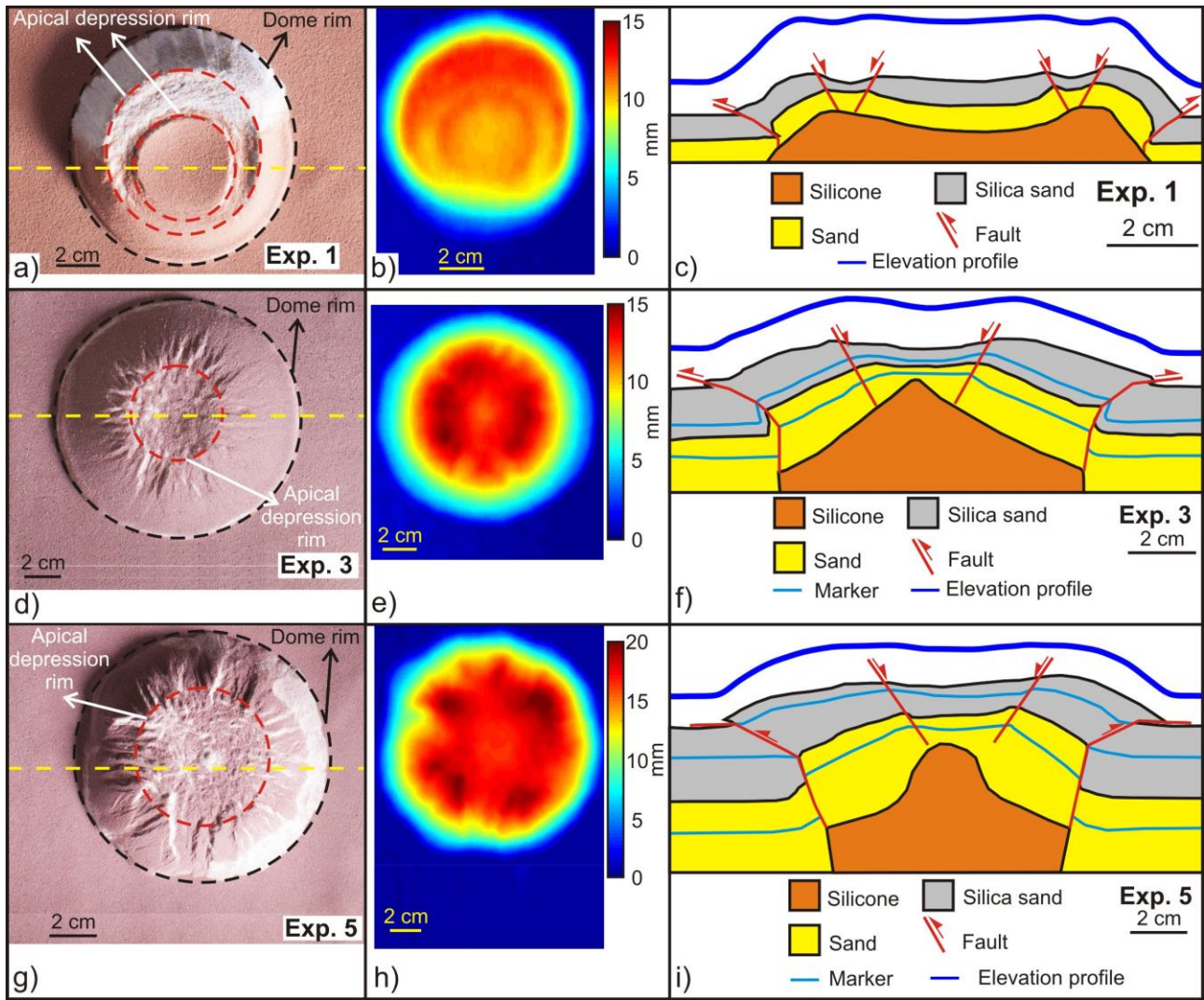
654

655

656

657

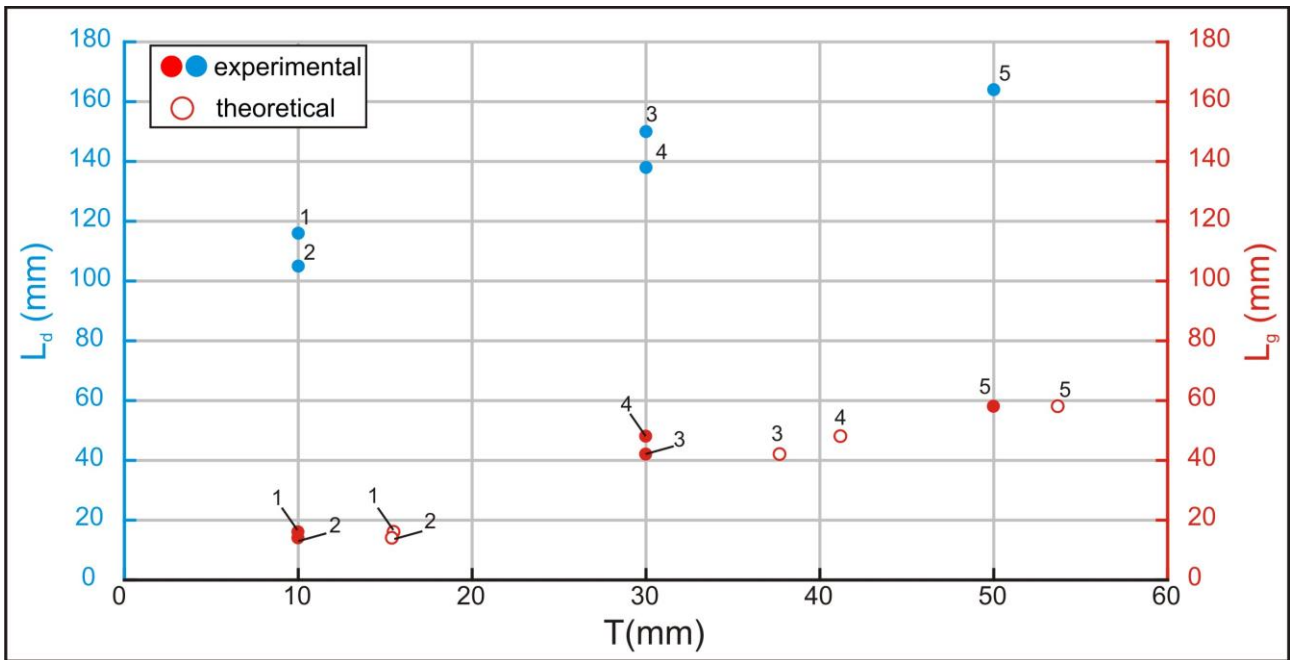
**Figure 6:** a) Panoramic view of the Arroyo Grande fault scarp showing the unaltered Cuicuiltic Member covering the altered and faulted ignimbrite and lavas (site LH-09). b) Normal fault affecting the altered ignimbrite deposits unconformably covered by the post-caldera, unaltered Cuicuiltic Member deposits (LH-09). Note that the Cuicuiltic Member deposits are not faulted at this location; the fault can be thus considered as a fossil fault with respect to the Cuicuiltic Member deposition. c) Block of altered trachyandesite buried by unaltered Cuicuiltic Member layers along the Maxtaloya fault scarp. d) Los Humeros fault scarp (LH-10) induced by the ascent of the trachyandesitic extrusion on top of the fault plane. e) Trachyandesite plug cropping out ~150 southward the fault scarp shown in d) (indicated by the red arrow). f) Jointing and alteration of the Cuicuiltic Member within the apical depression of the Loma Blanca dome (LH-01). g) Equal-area stereo-plot of the attitudes of faults and fractures in all the structural outcrops.



658  
 659  
 660  
 661  
 662  
 663  
 664  
 665  
 666  
 667  
 668  
 669  
 670  
 671  
 672  
 673  
 674  
 675  
 676

**Figure 7:** a) d) g) Top view image of the experiments 1, 3 and 5. b) e) h) cumulative vertical displacement; colour scale is proportional to the amount of uplift. c) f) i) Drawing of the cross section view obtained after cutting the section close to the dome center. The elevation profiles are obtained from laser scanner data. The yellow dashed line in a) d) g) indicates the trace of the section views and of the elevation profiles.



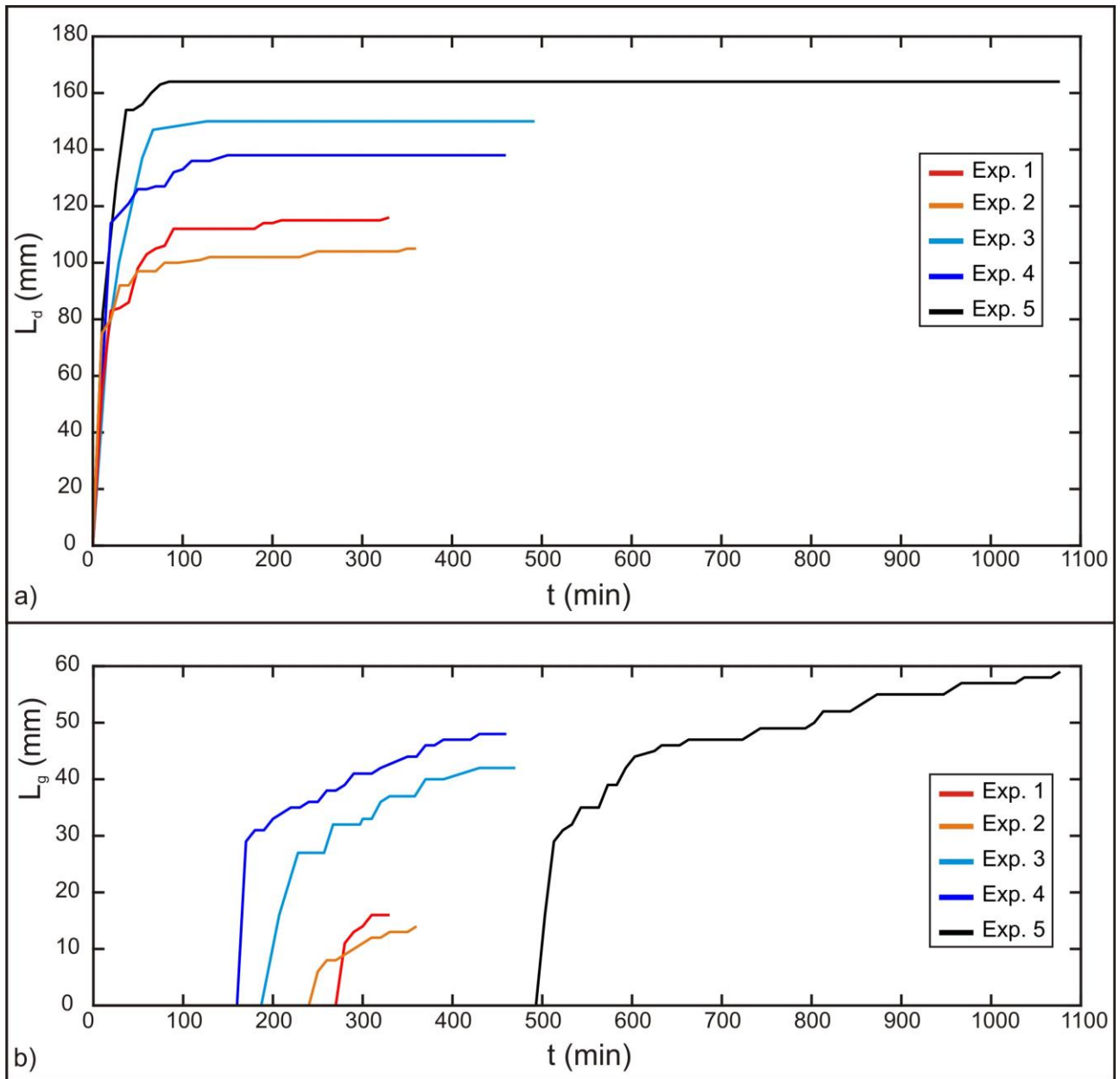


677

678

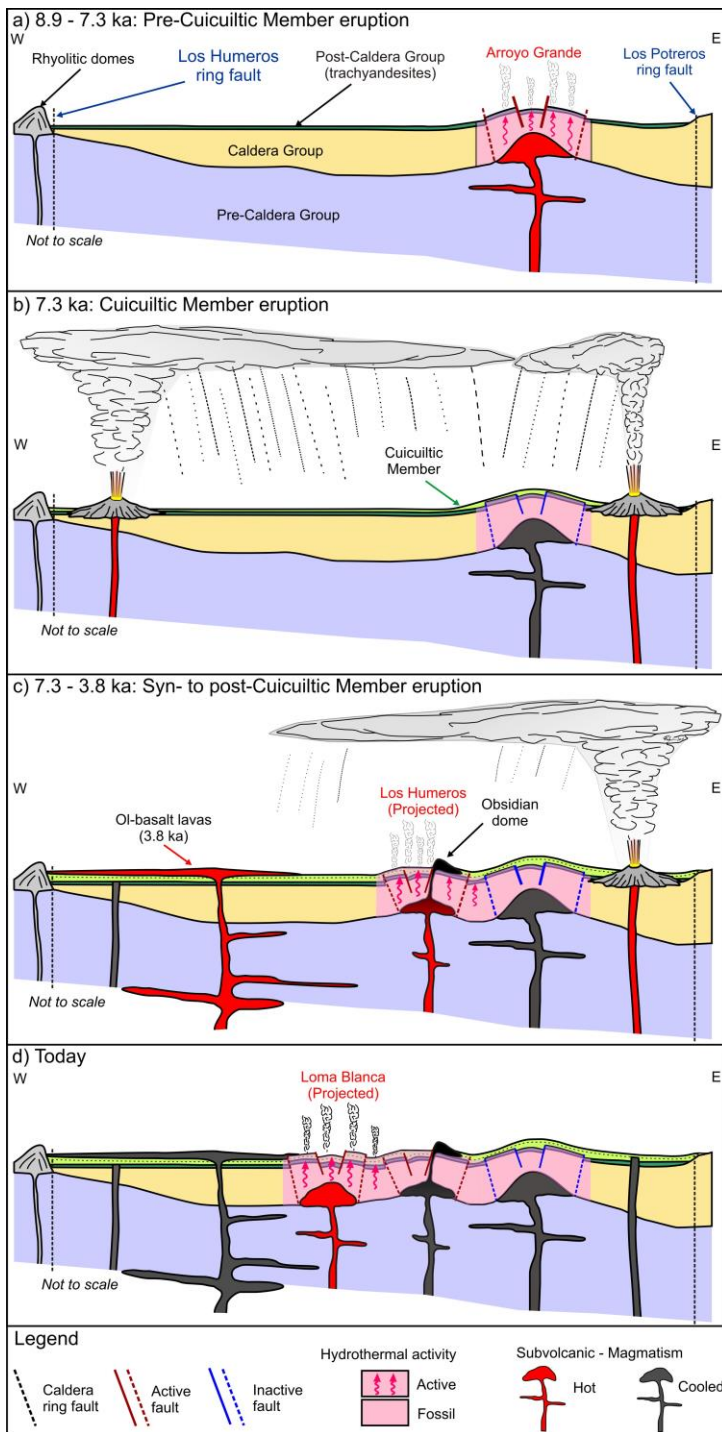
679

**Figure 8:  $L_g$  (apical depression width) and  $L_d$  (dome diameter) versus  $T$  (overburden thickness). Theoretical values calculated after equation 1 (see discussion section). The numbers above each point indicate the experiment number.**



680  
 681 **Figure 9: a) Time evolution of the dome diameter ( $L_d$ ). b) Time evolution of the apical depression width ( $L_g$ ). Both  $L_d$  and  $L_g$**   
 682 **show a similar evolution trend with a first stage of abrupt increase at the beginning of each experiment. In the second stage**  
 683  **$L_d$  becomes constant at  $t \sim 90$  min (experiments 1-2-3),  $t \sim 150$  min (experiment 4) and  $t \sim 65$  min (experiment 5) while  $L_g$**   
 684 **increases slightly from  $t \sim 250$ -280 min (experiments 1-2),  $t \sim 210$  min and  $\sim 170$  min (experiments 3 and 4) and  $t \sim 530$  min**  
 685 **(experiment 5) till the end of the experiment.**

686  
 687  
 688  
 689  
 690  
 691  
 692  
 693  
 694  
 695



696

697

698

699

700

701

702

703

704

705

706

707

**Figure 10: Schematic model of the evolution of the sub-surface structure of the Los Potreros caldera floor. Multiple magmatic intrusions located at relatively shallow depth (< 1 km) are responsible for the localized bulging of the caldera floor (Loma Blanca, Los Humeros and Arroyo Grande uplifted areas). a) Pre Cuicuiltic Member eruption: emplacement of a felsic intrusion at shallow depth and formation of the Arroyo grande bulge characterized by extensional faulting at its top, reverse faulting at its base and hydrothermalism. b) Cuicuiltic Member eruption: eruption of the Cuicuiltic Member covering the hydrothermally altered post-caldera trachyandesitic lavas. c) Syn to post Cuicuiltic Member eruption: formation of the Los Humeros fault and extrusion of obsidian lava domes along the fault scarp. As the trachyandesitic domes are covered with Cuicuiltic Member only at his base, the lava extrusion occurred during and post the Cuicuiltic Member eruption. d) Formation of the Loma Blanca bulge with the current hydrothermal activity and extensional faulting occurring within the apical depression. Notice that the emplacement of the successive most recent domes (Los Humeros and Loma blanca) are not aligned on the same plane, they are shown for practical purposes.**

Stage	Age (ka)	Main stratigraphic units
Post-caldera	< 69	Cuicuiltic Member and trachyandesitic to basaltic lavas
		Llano Tuff
		Xoxoctic Tuff
		Rhyolitic domes
Caldera	164-69	Zaragoza ignimbrite
		Faby Tuff
		Xaltipan ignimbrite
Pre-Caldera	700-164	Rhyolitic Domes

708 Table 1 Summary of the main stratigraphic units of the three evolutionary stages of the Los Humeros Volcanic complex  
709 (Carrasco-Núñez et al., 2017b, 2018).

Parameter	Definition	Value (experiments)	Value (nature)
T	Thickness of the overburden	1-5 X 10 <sup>-2</sup> m	300-2000 m
L <sub>d</sub>	Dome diameter	1-1.6 X 10 <sup>-1</sup> m	2000 m
H	Dome height	1.1-2 X 10 <sup>-2</sup> m	100 m
ρ <sub>s</sub>	Density of brittle overburden	1400 kg/m <sup>3</sup>	2800 kg/m <sup>3</sup>
φ	Angle of internal friction	35°	25-40°
τ <sub>0</sub>	Cohesion (brittle overburden)	300 Pa	10 <sup>6</sup> Pa
ρ <sub>m</sub>	Density of intrusive material	1000 kg/m <sup>3</sup>	2500 kg/m <sup>3</sup>
μ <sub>m</sub>	Viscosity of intrusive material	10 <sup>4</sup> Pa s	10 <sup>15</sup> Pa s
g	Gravity	9.8 m/s <sup>2</sup>	9.8 m/s <sup>2</sup>
t	Timespan for deformation	2.8-6.5 X 10 <sup>4</sup> s	1.9 X 10 <sup>12</sup> s

710 Table 2. Comparison of the geometric and material properties parameters of the experiments and nature.

Dimensionless ratio	Experiments	Nature
Π <sub>1</sub> = T/L <sub>d</sub>	0.1-0.5	0.15-1
Π <sub>2</sub> = H/L <sub>d</sub>	0.08-0.2	0.05-0.1
Π <sub>3</sub> = ρ <sub>s</sub> /ρ <sub>m</sub>	1.4	1.12
Π <sub>4</sub> = φ	35	25-40
Π <sub>5</sub> = ρ <sub>m</sub> H <sup>2</sup> /μ <sub>mt</sub>	6.1 X 10 <sup>-10</sup>	1.3 X 10 <sup>-20</sup>
Π <sub>6</sub> = ρ <sub>m</sub> gHt/μ <sub>m</sub>	1.3 X 10 <sup>3</sup>	4.6 X 10 <sup>3</sup>
Π <sub>7</sub> = ρ <sub>s</sub> gT/τ <sub>0</sub>	2.3	8.24

711 Table 3. Definition and values of the dimensionless ratios Π in nature and in the experiments.

Exp	T (mm)	L <sub>g</sub> (mm)	L <sub>d</sub> (mm)	θ	α	T <sub>t</sub> (mm)	σ (%)
1	10	16	116	58°	14°	15.5	55
2	10	14	105	63°	27°	15.4	54
3	30	42	150	58°	14°	37.7	27
4	30	48	138	56°	18°	41.2	37
5	50	58	164	58°	21°	53.7	7

712 Table 4. Measured (L<sub>g</sub>, L<sub>d</sub>, θ, α) and imposed (T) parameters in the experiments. T=overburden thickness; L<sub>d</sub>= dome  
713 diameter; L<sub>g</sub>= apical depression width; θ= apical depression fault dip; α= dome flank mean dip; T<sub>t</sub>= theoretical overburden

714 thickness calculated with equation 1 (Brothelände and Merle, 2015, see discussion section);  $\sigma$ = percentage difference between  
715 T and  $T_c$ .